Remote Sensing of Atmospheric Aerosols and Trace Gases by Means of Multifilter Rotating Shadowband Radiometer. Part I: Retrieval Algorithm

MIKHAIL D. ALEXANDROV

Department of Applied Physics and Applied Mathematics, Columbia University, and NASA Goddard Institute for Space Studies, New York, New York

ANDREW A. LACIS AND BARBARA E. CARLSON

NASA Goddard Institute for Space Studies, New York, New York

BRIAN CAIRNS

Department of Applied Physics and Applied Mathematics, Columbia University, and NASA Goddard Institute for Space Studies, New York, New York

(Manuscript received 15 December 2000, in final form 6 July 2001)

ABSTRACT

A retrieval algorithm for processing multifilter rotating shadowband radiometer (MFRSR) data from clear and partially cloudy days is described and validated. This method, while complementary to the Langley approach, uses consistency between the direct normal and diffuse horizontal measurements combined with a regression technique to simultaneously retrieve daily time series of column mean aerosol particle size, aerosol optical depth, NO_2, and ozone amounts along with the instrument's calibration constants. Comparison with the traditional Langley calibration method demonstrates two advantages of the approach described here: greater calibration stability and a decreased sensitivity of retrievals to calibration errors.

1. Introduction

Aerosols, through their direct and indirect radiative forcing, are thought to be the largest source of uncertainty in defining the anthropogenic contribution to global radiative forcing of climate during the past century, and of the projected forcing of future climate change (Charlson et al. 1992; Hansen et al. 1995, 1997, 2000). Sulfate aerosols, in particular, with their negative forcing, are the most likely explanation of the discrepancy between modeled changes in global surface temperature and the observed temperature record (Kiehl and Rodhe 1995; Meehl et al. 1996; Tegen et al. 1996).

While global coverage is only possible with satellites, satellite aerosol retrievals are complicated by sun–satellite geometry effects, the need to separate the light reflected from the surface from that scattered by the aerosols, and the dependence of scattered light on particle shape. Due to the difficulty of separating surface and aerosol effects, most currently available satellite aerosol retrievals are for ocean only, where the relatively dark surface contributes little to the observed intensity. Measurements by current state-of-the-art sensors, such as moderate resolution imaging spectroradiometer (MODIS) and multiangle imaging spectroradiometer, (MISR) will improve the reliability of retrievals over ocean and extend detection to land areas. However, this does not reduce the importance of ground-based (and especially network) measurements, which are required to validate the satellite retrievals and provide a more complete picture of the nature of the aerosol.

Toward this end we have focused on the development of retrieval algorithms (Alexandrov et al. 1999a) for the multifilter rotating shadowband radiometer (MFRSR). The key advantages of this instrument are its automated operation and relatively low cost, allowing the construction of networks. This together with their growing international use makes the MFRSR a potentially important tool for climate research. The algorithm presented in this paper emphasizes the network applications of this instrument, rather than focusing on data derived from campaigns or intensive operation periods where additional correlative measurements are available. As such, the algorithm is structured so that no external measurements are required for the retrievals (since they may not be available at all network sites), and the instrument's calibration is determined directly from the

Corresponding author address: M. Alexandrov, NASA Goddard Institute for Space Studies, 2880 Broadway, New York, NY 10025. E-mail: malexandrov@giss.nasa.gov

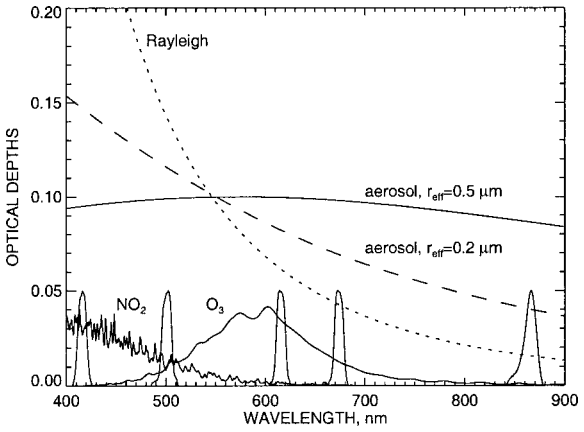

FIG. 1. Typical optical depths of atmospheric constituents in the MFRSR spectral region: Rayleigh (at 1013.25-mb pressure); aerosols with $r_{\text{eff}} = 0.2$ and 0.5 ($v_{\text{eff}} = 0.2$, gamma distribution) and $\tau_a = 0.1$ at 550 nm; NO_2 (2-DU column amount); and ozone (300-DU column amount). Water vapor and O_2–O_2 absorption are not shown because they do not affect measurements in MFRSR spectral channels. The instrument spectral response functions (in arbitrary units) are depicted for the first five channels (415–870 nm).

data, eliminating instrument downtime for calibration. This leads to a more homogeneous data record and potentially reduces the expense of network operations.

The MFRSR makes precise simultaneous measurements of the direct solar beam extinction and horizontal diffuse flux, at six wavelengths (nominally 415, 500, 615, 670, 870, and 940 nm) at 1-min intervals throughout the day [Wesely 1982, cf. Harrison et al. (1994) for a description of the operational details, and Schmid et al. (1999) for comparison with other instruments]. Besides water vapor at 940 nm, the other gaseous absorbers within the MFRSR channels are NO_2 (at 415, 500, and 615 nm) and O_3 (at 500, 615, and 670 nm). Aerosols and Rayleigh scattering contribute atmospheric extinction in all MFRSR channels.

Since there is no way to couple the 940-nm channel measurements with the 415–870-nm measurements, we leave all discussion of water vapor to a later paper and focus on the first five MFRSR channels. Typical spectral optical depths for NO_2 (Merienne et al. 1995; Schneider et al. 1987) and O_3 (E. P. Shettle 1997, personal communication) are shown in Fig. 1 along with the spectral extinction provided by Rayleigh scattering and aerosols. Aerosol spectral extinction is calculated (for given refractive index and particle size) using Mie theory. The effects of particle nonsphericity are neglected because the difference in the extinction cross section between nonspherical and spherical particles is roughly $\pm 1\%$ (Mishchenko et al. 1997).

Thus, provided that the spectral optical depths are accurately measured, the filter response functions and calibrations are accurately known, the unique spectral signature of each atmospheric constituent permits the retrieval of daily time series of aerosol optical depth and effective radius, as well as NO_2 and O_3 column amounts by a variety of techniques [e.g., brute force least squares fitting (Lacis et al. 1996)].

Factors influencing the calibration of a sun photometer include stability of the filter spectral response function, filter transmission, and knowledge of the extraterrestrial solar spectrum (cf. Schmid et al. 1998). Extensive laboratory recalibrations have shown that the spectral response of the filters are stable but that their transmission changes with time, hence the need for calibration. Since there are calibration issues with standard lamps (cf. Michalsky et al. 1996), it is preferable to determine the instrument calibration from the measurements. Traditionally, this is done via Langley regression at high-altitude sites (cf. Holben et al. 1998; Schmid et al. 1997, 1998), however, since filter transmission can change at any time (i.e., between high-altitude calibrations) it is preferable to develop alternative techniques. One approach developed by Harrison and Michalsky (1994) is to average the calibration coefficients determined from Langley analysis over 20–40 clear days within a roughly 3-month window to determine an accurate calibration. Potential time-dependent changes in filter transmission require that the calibration be checked for every period of operation. Comparison of aerosol optical depths retrieved from solar radiometers (Schmid et al. 1999) confirmed the accuracy of this type of calibration approach for the MFRSR through comparison with instruments calibrated at Mauna Loa.

Once the calibration is known, it is possible to retrieve aerosol properties and column gas amounts from the spectral dependence of the measured extinction. Techniques have been developed to retrieve aerosol optical depths (e.g., King and Byrne 1976) and an estimation of aerosol particle size based on the spectral dependence of aerosol extinction (King et al. 1978; Lacis et al. 1996). Direct and diffuse ratios have been used to determine aerosol single scattering albedo as well as surface albedo (Herman et al. 1975; King 1979). Alternatively, aerosol optical depth can be determined from the direct to diffuse ratio under certain assumptions of aerosol absorption and surface albedo (O'Neill et al. 1989); however, the sensitivity of these retrievals to modeling assumptions needs to be studied in order to estimate the accuracy of the retrieval product. The advantage of the latter approach is that no calibration is required.

In our approach, we use the direct to diffuse ratios as an independent source of information (since both quantities are measured with the same detector) with which to correct the direct beam optical depth. Alternative calibration techniques using diffuse radiation have been developed by Tanaka et al. (1986) and used by Nakajima et al. (1996) for the case where the angular dependence of the solar intensity is measured.

In this paper we present an algorithm that provides retrieval of aerosol properties and NO_2 and O_3 column amounts together with the simultaneous determination of the instrument calibration constants. The algorithm

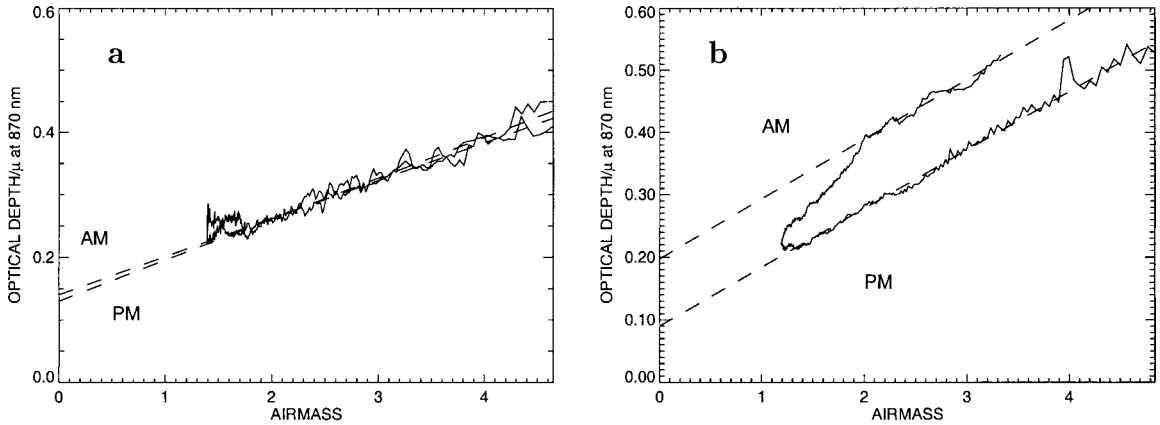

FIG. 2. (a) Langley plot for the 870-nm channel data obtained on 1 Oct 1996 in NYC; (b) inconclusive Langley plot for the same channel and site (2 Sep 1996).

consists of two basic steps: 1) consistency between the direct normal and diffuse horizontal measurements in the fifth (870 nm) channel, and 2) a regression technique to retrieve daily time series of column mean aerosol particle size, aerosol optical depth in all channels, NO_2, and ozone column amounts together with calibration of the first four channels.

In the following sections we present our algorithm (section 2) and compare the results of our retrievals with other measurements (section 3). Finally, we discuss the current status of our retrieval algorithm as well as current applications. Additional analysis results are presented in our companion paper (Alexandrov et al. 2002).

2. Method

The first step in our algorithm consists of using the consistency between the direct normal and diffuse horizontal measurements in the fifth channel (870 nm) to determine the aerosol optical depth and calibration constant for this channel. This channel is optimal for this purpose since the extinction source is primarily aerosol with little contribution from gaseous absorbers. Since the direct and diffuse irradiances are measured with the same detector, the difference between the optical depth derived from the uncalibrated direct beam measurement and that inverted from the calibration-independent ratio of the direct and diffuse intensities is considered the calibration effect. The effect of the so-called clear-sky direct to diffuse discrepancy, an overestimation of the diffuse irradiance by radiative transfer models that use as inputs the optical parameters obtained from the direct beam measurements (cf. Halthore et al. 1998; Halthore and Schwartz 2000), on this procedure requires some modifications as described below.

The second step consists of using a regression technique to retrieve daily time series of column mean aerosol particle size, aerosol optical depth in all channels, NO_2, and ozone column amounts together with the calibration constants for the first four channels. The primary advantages of this approach are the spectral consistency of the calibration procedure and the coupling of the calibration and retrieval processes.

a. Basic notions

The direct solar beam irradiance measured by the MFRSR at each time step in *i*th spectral channel can be represented in the form,

$$I_i = C_i I_i^0 \exp\left(-\frac{\tau_i}{\mu}\right), \tag{1}$$

where μ is the inverse of the airmass (essentially equal to the cosine of the solar zenith angle), τ_i is the atmospheric column extinction optical depth corresponding to the *i*th channel, and I_i^0 are the top of the atmosphere solar intensities. This means that we take the lamp-calibrated intensities and determine correction factors C_i to the calibration used. The original (lamp) calibration is used only for a rough conversion of counts into watts per meters squared.

The optical depths τ_i can be expressed from (1) as

$$\tau_i = -\ln\left(\frac{I_i}{I_i^0}\right) \cdot \mu - c_i\mu. \tag{2}$$

Here we introduce the notation

$$c_i = -\ln C_i. \tag{3}$$

In the following we use the term ''calibration coefficients'' for the coefficients c_i.

We will also use the notation $\tilde{\tau}_i$ for the uncalibrated optical depths:

$$\tilde{\tau}_i = -\ln\left(\frac{I_i}{I_i^0}\right) \cdot \mu = \tau_i + c_i\mu. \tag{4}$$

In this notation a Langley plot is the plot of $\tilde{\tau}_i/\mu$ versus air mass $(1/\mu)$. Examples of such plots are shown in Fig. 2. By assuming stability of τ during the morning

and afternoon periods with air masses higher than two and approximating the curves in Fig. 2 with straight lines for these periods, estimates of the calibration coefficient c_i can be obtained as the intercepts of the corresponding lines. However, when aerosol optical depth changes (Fig. 2b), the Langley technique cannot be used to determine the calibration.

The contribution of the Rayleigh scattering is accurately known. We use

$$\tau_R(\lambda) = 0.008\,569\lambda^{-4}(1 + 0.0113\lambda^{-2} + 0.000\,13\lambda^{-4})\frac{P}{P_0}, \quad (5)$$

where λ is the wavelength in micrometers, P is atmospheric pressure in millibars, and $P_0 = 1013.25$ mb is the standard pressure (Hansen and Travis 1974) to remove the Rayleigh contribution from each channel before we begin. This formula has been shown to produce good agreement with exact calculations (Teillet 1990) and be consistent with the results of Bodhaine et al. (1999) for the spectral range of interest. Thus, in the following, $\tilde{\tau}_i$ refers to optical depths with the Rayleigh contribution subtracted.

Finally, it is necessary to select the data or data interval that is appropriate for analysis. While we have developed several automated cloud-screening procedures, based on the spectral behavior and temporal variability of cloud extinction, we have manually selected the clear intervals on partially cloudy days for this analysis using an interactive program that allows us to edit the data interval to ensure that we are not including thin cirrus.

Once we have selected the data interval for analysis we proceed with the retrieval algorithm, which consists of the following steps: 1) determination of the calibration coefficient and aerosol optical depth in the fifth channel (870 nm), 2) analytical solution of a system of linear (in aerosol optical depth and gas column amounts) equations to retrieve the aerosol size distribution parameters and the aerosol optical depths for all five channels, 3) retrieval of the NO_2 and ozone column amounts (together with the calibration coefficients in the first two channels), and 4) determination of the calibration coefficients in the first five channels.

b. *Calibration using direct-to-diffuse ratios and determination of 870-nm channel optical depth*

Direct to diffuse ratios present a source of information that is independent of instrumental calibration, provided that both the direct and diffuse intensities are measured with the same detector. The following factors contribute to the diffuse radiation under cloud-free conditions: aerosol optical depth, particle size, and single scattering albedo as well as surface albedo and Rayleigh scattering. In the case of absorbing aerosol, its vertical profile is important as well. Variations of real part of the aerosol refractive index within a typical natural range (1.3–1.6) do not play a significant role (King and Herman 1979). In our algorithm we restrict our use of the diffuse flux measurements to the 870-nm channel since this is the only channel not notably affected by ozone and/or NO_2 absorption, hence the diffuse intensity does not depend on the unknown vertical distribution of these gases.

In a vertically inhomogeneous atmosphere the optical depth derived from the direct beam and diffuse horizontal measurements are not identical since the optical depth determined from the diffuse measurement using a plane-parallel multiple scattering model is an average over all angles. Hence, in comparison with the direct beam optical depth the diffuse optical depth is smoother and changes slower as a function of time than the optical depth derived from the direct beam.

Diffuse flux measurements provide information on both aerosol absorption and the instrument's calibration. Differences in the solar zenith angle dependence of these two effects suggests that they should be separable provided that the aerosol composition is stable over the day and sufficient clear periods exist in the datasets. However, determination of the aerosol single scattering albedo from comparisons between direct and diffuse measurements is problematic (at least for low-altitude sites), because of a clear-sky direct to diffuse discrepancy issue. This discrepancy is an overestimation of diffuse irradiance by radiative transfer models that use as inputs the optical parameters obtained from the direct beam measurements (Kato et al. 1997; Halthore et al. 1998; Halthore and Schwartz 2000). Our modeling of the diffuse beam (assuming conservative scattering) shows that the optical depths inverted from direct to diffuse ratios cannot match the uncalibrated direct beam optical depths solely through the addition of a calibration term. Some additional opacity, with an average optical depth of 0.02, seems to be missing from the diffuse measurements. This discrepancy can be resolved by assuming an unphysical aerosol single scattering albedo of about 0.5. This complicates the retrieval of a physically plausible aerosol single scattering albedo, since real aerosol absorption cannot be separated from the ''anomalous'' one. In the present work we do not attempt to solve the direct to diffuse discrepancy, instead we use the observed stability of the missing opacity (it appears to be nearly constant not only during the day but also for periods of several months) to improve the direct–diffuse calibration procedure. The stability of the missing opacity allows us to apply Langley-like regressions to the difference between direct beam and direct–diffuse ratio optical depths to obtain the instrument's calibration constant. The validity of this approach has been tested on an exceptionally clear dataset from Davis, California. As described in section 3a, our calibrations agree with those from reliable Langley regressions, while our regression technique is shown to be more conclusive than the ordinary Langley approach for the most of the days studied.

To model the diffuse flux, we perform multiple scattering calculations using the doubling and adding method (Hansen and Travis 1974) with a Henyey–Greenstein phase function. The spectral dependence of aerosol extinction is calculated using Mie theory assuming nonabsorbing aerosol ($n_r = 1.4$, $n_i = 0$). King et al. (1978) have shown that aerosol spectral extinction does not significantly vary with aerosol absorption for $n_i \leq 0.03$. We investigated the sensitivity to phase function by comparing the Henyey–Greenstein results with those obtained using a full Mie phase function, confirming the fact that retrieval results are not sensitive to the particular functional shape of the phase function. Finally, we run the direct–diffuse calibration procedure in two iterations. As a first guess, we assume an asymmetry parameter of 0.75 then determine the actual particle size by the method described below, and then rerun the calibration routine with the new asymmetry parameter thereby iteratively correcting the calibration coefficient determined in the first step. The effect of aerosol absorption is to alter the direct–diffuse ratio resulting in overestimation of the calibration coefficient and underestimation of aerosol optical depth.

The retrievals are substantially simplified by using the analytical relationship between the direct to diffuse ratio $\Phi = I_{\text{dir}}/I_{\text{dif}}$ and the surface albedo (King and Herman 1979):

$$A = \frac{1}{R}\left(\frac{1 - (\Phi/\Phi_0)}{1 + \Phi \cos\theta}\right), \tag{6}$$

where A is the surface albedo; Φ is the direct to diffuse ratio corresponding to this albedo; and Φ_0 to zero surface reflectivity, respectively; and where $R = R(\tau)$ is the reflection function integrated over all scattering angles; and θ is the solar zenith angle. It is important to note that I_{dir} and I_{dif} are measured using the same spectral filter and detector, thus the calibration constant is cancelled in the ratio Φ.

Figure 3 shows that this calibration procedure works even for days with highly variable optical depth. For many of these days the retrieval of other parameters is impossible, but the optical depth in the 870-nm channel can be estimated. Although the surface albedo is an unknown quantity, the retrieved aerosol optical depth depends only weakly on its assumed value: a reasonable assumption of $0 < A < 50\%$ results in the uncertainty of ± 0.01 (shown by shaded area in Fig. 3) in the optical depth inverted from (6). Analytical estimates of the errors caused by the uncertainty in surface albedo were also performed by O'Neill et al. (1989). The method is certainly not applicable in the presence of strong side reflections from clouds and/or bright objects affecting the diffuse irradiance measurements. However, periods with these conditions can be easily detected from the data and removed from the analysis.

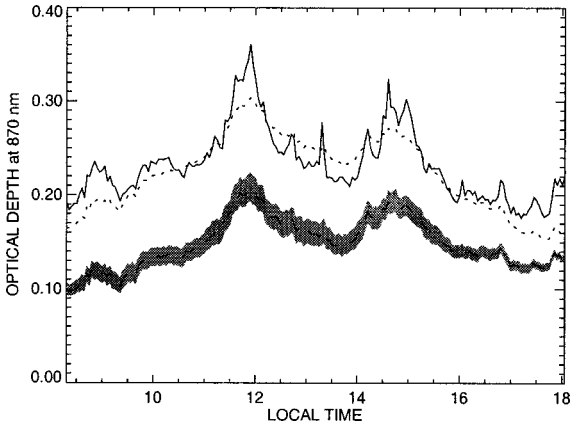

FIG. 3. Optical depths at 870 nm (7 Jun 1996, NYC). Solid curve depicts uncalibrated optical depth from direct beam. Calibration-independent but smoothened optical depth from direct-to-diffuse ratio, inverted under assumption of the ground albedo being within 10% to 50% is shown by the shaded area. The optical depth corresponding to the ground albedo of 30% is plotted as a dashed curve inside this area. The latter optical depth with calibration (proportional to μ) and the appropriate offset added to match the optical depth from the direct beam is represented by the dotted curve.

c. Regression method for determination of aerosol extinction

The conventional Langley technique does not yield accurate results when aerosol optical depth is changing systematically during the day. However, as shown below, in such cases aerosol spectral extinction properties (determined by composition and particle size distribution) appear to be more stable. Here we describe a new regression technique that is similar to the Langley approach but relies on the spectral stability of aerosol extinction instead of optical depth stability. Philosophically similar methods were introduced by Forgan (1994) and Soufflet et al. (1992) in order to reduce uncertainties in calibration. However the present method is somewhat different both conceptually and in its practical applications.

The a priori reason for assuming stability in aerosol extinction rather than optical depth is that most of the optical depth variability stems from transport. An aerosol ''cloud'' consisting of particles having the same origin, composition, and size distribution may have a complicated horizontal distribution, which induces high optical depth variability when this cloud passes over a sun photometer. Support for the greater stability of aerosol extinction is found in the regression plots shown in Figs. 4a and 4b that appear to be much closer to a straight line (i.e., the same for the whole day) than the Langley plot for the same day (previously shown in Fig. 2b). Note that these plots are linear when the spectral shape of aerosol extinction does not change, while the optical depth may arbitrarily vary.

In the problem at hand (after the Rayleigh terms are removed), the measured quantities and the quantities to

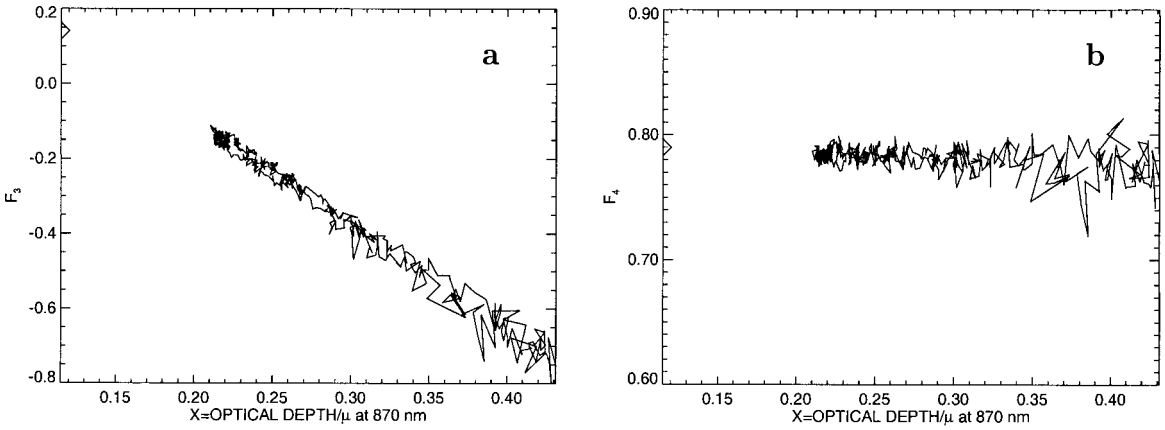

FIG. 4. (a) Aerosol extinction regression plot: F_3 vs x, diamond depicts the calibration point (c_5, A_3); (b) same as (a), but for F_4.

be determined satisfy the following system of five equations:

$$\tilde{\tau}_1 = q_1\tau_a + \beta_1 x_{NO_2} + c_1\mu, \tag{7}$$

$$\tilde{\tau}_2 = q_2\tau_a + \beta_2 x_{NO_2} + \gamma_2 x_{O_3} + c_2\mu, \tag{8}$$

$$\tilde{\tau}_3 = q_3\tau_a + \beta_3 x_{NO_2} + \gamma_3 x_{O_3} + c_3\mu, \tag{9}$$

$$\tilde{\tau}_4 = q_4\tau_a + \beta_4 x_{NO_2} + \gamma_4 x_{O_3} + c_4\mu, \quad \text{and} \tag{10}$$

$$\tilde{\tau}_5 = \tau_a + c_5\mu. \tag{11}$$

Here, $\tilde{\tau}_i$ is the measured optical depth in the ith channel [Eq. (4)]; $q_i = Q^i_{ext}/Q^5_{ext}$ is the Mie-scattering extinction ratio normalized to the fifth (870 nm) channel (by definition $q_5 = 1$); β_i and γ_i are the effective spectral absorption coefficients for NO_2 and O_3, respectively, weighted by the solar flux and filter response function of each respective MFRSR channel (the coefficients β_5, γ_1, and γ_5 are effectively equal to zero); x_{NO_2} and x_{O_3} are respective column amounts of NO_2 and ozone; τ_a is the aerosol optical depth in MRFSR channel 5 (at 870 nm), and c_i are the calibration coefficients [Eq. (3)].

In modeling gaseous absorption we use the room temperature absorption cross-sections for NO_2 measured by Merienne et al. (1995) for wavelengths below 500 nm and by Schneider et al. (1987) for wavelengths above 500 nm. The absorption cross sections for ozone (a reference temperature of 220 K is used) were obtained from E. P. Shettle (1997, personal communication), they are based on the measurements of Anderson and Mauersberger (1992) and Burkholder and Talukdar (1994). The absorption cross-sections for NO_2 and ozone have recently been reviewed and compared with those obtained using the Global Ozone Monitoring Experiment (GOME) flight model (FM) spectrometer. Burrows et al. (1998) find that the average difference between the Merienne et al. (1995) cross sections and the GOME results is smaller than 2%. The cross-sections measured by Schneider et al. (1987) are on average 1%–4% smaller than those measured by the GOME spectrometer. Given the uncertainty in our NO_2 retrievals introduced by ambiguities in the aerosol size distribution (described below), this level of accuracy is more than sufficient for our retrievals. In the 540–640-nm spectral range, our ozone coefficients are 2%–3% higher than those determined using the GOME FM spectrometer (Burrows et al. 1999).

In the above set of equations the explicit dependence on x_{NO_2}, and then on x_{O_3} can be eliminated. Then by substituting $\tau_a = \tau_5 - c_5\mu$, and dividing the expressions by μ, the following two equations can be obtained:

$$F_3 = B_3(x - c_5) + A_3, \quad \text{and} \tag{12}$$

$$F_4 = B_4(x - c_5) + A_4, \tag{13}$$

where we use the following notations:

$$x = \frac{\tilde{\tau}_5}{\mu}, \tag{14}$$

$$F_i = \mu^{-1}[\tilde{\tau}_i - b_{i1}\tilde{\tau}_1 - g_{i2}(\tilde{\tau}_2 - b_{21}\tilde{\tau}_1)], \tag{15}$$

$$B_i = q_i - b_{i1}q_1 - g_{i2}(q_2 - b_{21}q_1), \tag{16}$$

$$A_i = c_i - b_{i1}c_1 - g_{i2}(c_2 - b_{21}c_1), \tag{17}$$

and $i = 3, 4$. In the above, $b_{ij} = \beta_i/\beta_j$ and $g_{ij} = \gamma_i/\gamma_j$ are the spectrally weighted NO_2 and O_3 absorption coefficient ratios, respectively. Note that the left-hand side F_i of the Eqs. (12) and (13) contain only measured parameters as expressed by (15) and can therefore be calculated directly from the observed data at each measurement time step (i.e., without any modeling assumptions). Meanwhile, the right-hand sides are linear functions of the argument $x = \tilde{\tau}_5/\mu$ over any time interval where the aerosol extinction parameters q_i do not change (note also that so far no assumptions have been made with respect to the aerosol size distribution).

It is seen from the system of Eqs. (12) and (13) that $F_i = A_i$ when extrapolated to the point $x = c_5$ for any value of B_i (here and below, $i = 3, 4$). Accordingly, the A_i represent combinations of calibration coefficients,

and are expected to remain constant during the day. The B_i being combinations of aerosol extinction ratios, may change in response to changes that may take place in aerosol spectral extinction due to variations in aerosol size or composition. Representative plots of F_i versus x for a typical clear day are shown in Figs. 4a and 4b. It follows from the above that all points on the plot $F_i(x)$ corresponding to the same aerosol size distribution belong to a straight line with slope B_i passing through the ''calibration point'' with the coordinates (c_5, A_i). This point, strictly speaking, must be located to the left of the plotted data, since otherwise the aerosol optical depth at 870 nm would have to be negative. Since we actually do not know which points belong to the same size mode, the calibration point cannot be found as the intersection of all such lines. Nevertheless, the general shape of the resulting plots $F_3(x)$ and $F_4(x)$ is such that knowing the x-coordinate c_5 of the calibration point (see the previous section), the values of its y-coordinate A_i can be determined from the condition of the minimal mean deviation of the corresponding functions $B_i(x) = [F_i(x) - A_i]/(x - c_5)$ from their mean values. This minimum is usually well pronounced; that is, the curves in Fig. 4 ''point'' to the calibration point.

After the calibration point is determined, the time series of the coefficients B_3 and B_4 [Eq. (16)] can be obtained. Note that B_i, being the slopes of the curves in Figs. 4a and 4b, can be estimated, without knowing c_5 by means of a Langley-like regression. This means that the retrievals of the aerosol spectral extinction properties cannot be significantly affected by calibration uncertainties in the aerosol optical depth determination of the previous step of the retrieval algorithm.

d. Retrieval of aerosol size and optical depth in all channels

In our case, the coefficients B_3 and B_4 being the combinations of the (unknown) aerosol extinction ratios q_i are the only available source of information about the aerosol size distribution. This means that one can generally determine no more than two parameters of the aerosol size distribution from this data. Thus, the direct inversion of the aerosol size distribution from the spectral data (King et al. 1978; Shaw 1979b, 1979c; Schmid et al. 1997; Dubovik and King 2000) is not appropriate for our purposes. We note however that our algorithm does not rely on external data sources, while in the cited papers the gas column amounts are either determined from other measurements or estimated from climatology.

It is formally possible to use the coefficients B_3 and B_4 to determine the effective radius r_{eff} and effective variance v_{eff} (cf. Hansen and Travis 1974) of an assumed aerosol size distribution. However, in practical applications, such retrievals are ambiguous because the measured optical depths cannot be uniquely explained with a combination of aerosol, ozone, and NO_2 contributions within the measurement accuracy of the MFRSR. This results in an interplay between aerosol size distribution parameters and NO_2 column amount such that one can simultaneously change the NO_2 column amount and the aerosol size distribution in such a way that the total optical depths in all channels remain unchanged. Fortunately, despite this ambiguity, both aerosols and atmospheric gases still can be characterized, but an accurate determination of the retrieval error bars is necessary for the retrieval products to be useful.

The formal procedure for determining the parameters of the assumed aerosol size distribution can be described as follows. First, Mie theory is used (specifying aerosol complex refractive index) to calculate the extinction ratios q_i for each pair of size distribution parameters. Then, the formulas [Eq. (16)] are applied to create look-up tables for B_3 and B_4 as functions of r_{eff} and v_{eff}. For each observed data point, these tables are used to construct level curves in the $(r_{\text{eff}}, v_{\text{eff}})$-plane corresponding to the values of B_3 and B_4 measured at this point. If these curves intersect, the coordinates of their intersection point are the r_{eff} and v_{eff} of the assumed aerosol size distribution at the time of the measurement. However, for real data no intersection or multiple intersections may occur. Typically, the level curves for B_3 and B_4 intersect only for a small fraction of measurements made during the day. The retrieved effective radii and variances exhibit high point-to-point variability, however, when plotted on the $(r_{\text{eff}}, v_{\text{eff}})$-plane they group tightly along the lines described above (Figs. 5b–d). This suggests a random character of the level curve intersections and their sensitivity to small errors in the measurements and calibrations which requires a modification to the retrieval approach.

We characterize the curve in Fig. 5a by the function $r_{\text{eff}}(v_{\text{eff}})$. This function can always be restored given the value of r_{eff} corresponding to the point of the curve where $v_{\text{eff}} = 0$ (actually, we take variance 0.01 to average out the Mie size parameter oscillations). We refer to this r_{eff} as to ''monodistribution radius'' since it is calculated under the assumption that all aerosol particles are effectively the same size. To quantify the dependence of our retrievals on the position of the $(r_{\text{eff}}, v_{\text{eff}})$-point on the curve, we perform all retrievals for five such points corresponding to $v_{\text{eff}} = 0.01$, 0.1, 0.2, 0.3, and 0.4. We use the difference between the retrievals for different v_{eff} to define the error bars due to uncertainties in the size distribution. These errors are typically negligible for ozone column amounts and long-wavelength aerosol optical depths. They are larger for NO_2 column amounts and short-wavelength aerosol optical depths due to the trade-offs between small particle and NO_2 extinction.

The time series of the monodistribution radius can be obtained either from B_3 or B_4 as functions of time (Fig. 6a). The values obtained from B_4 generally coincide with the ones derived from B_3, but are usually noisier, thus we use them primarily as a consistency check.

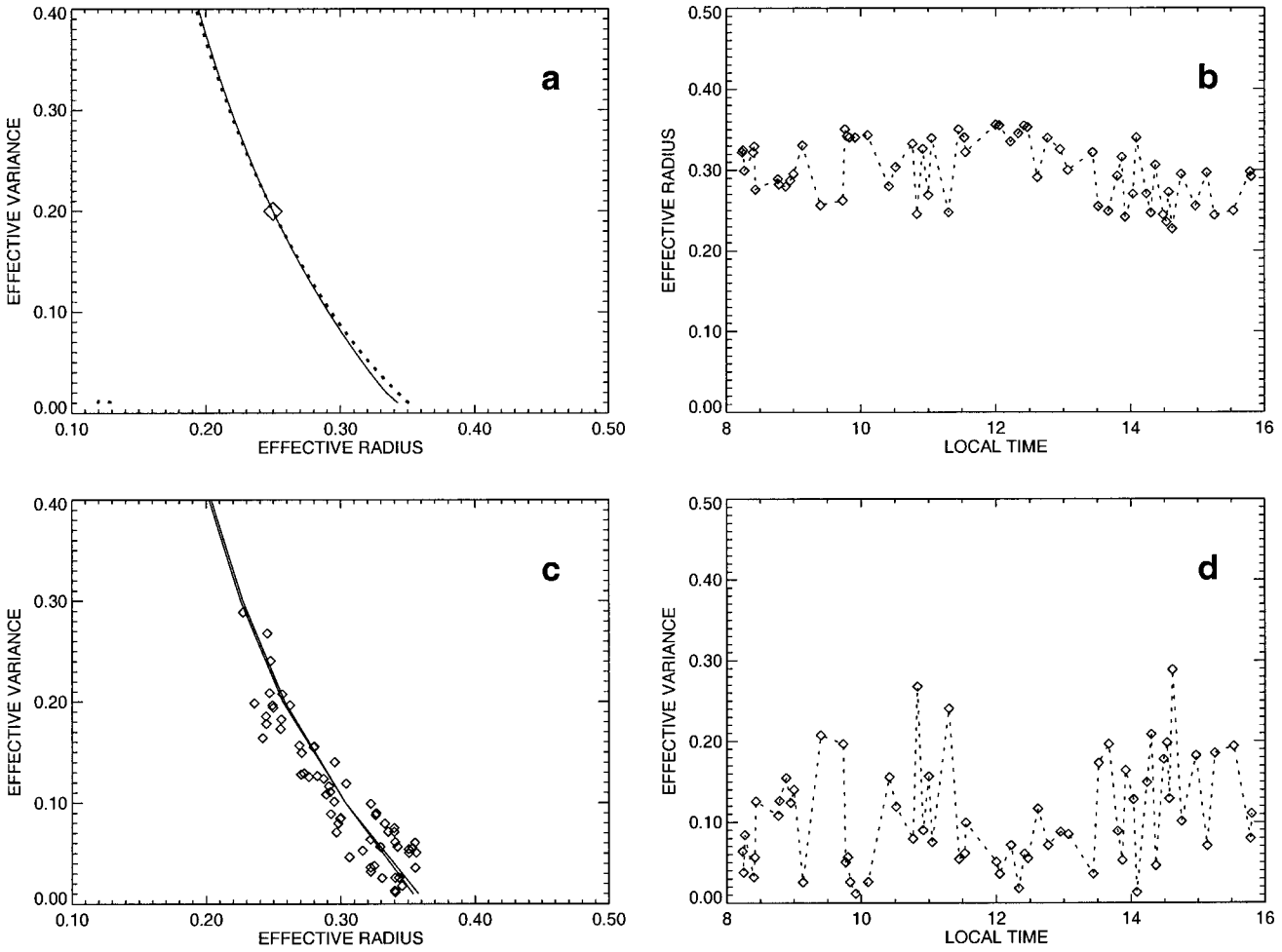

FIG. 5. (a) The level curves for B_3 and B_4 that nearly coincide; (b) time series of retrieved effective radii for NYC 2 Sep 1996; (c) time series of (d) plotted vs time series of (b); (d) time series of retrieved effective variances.

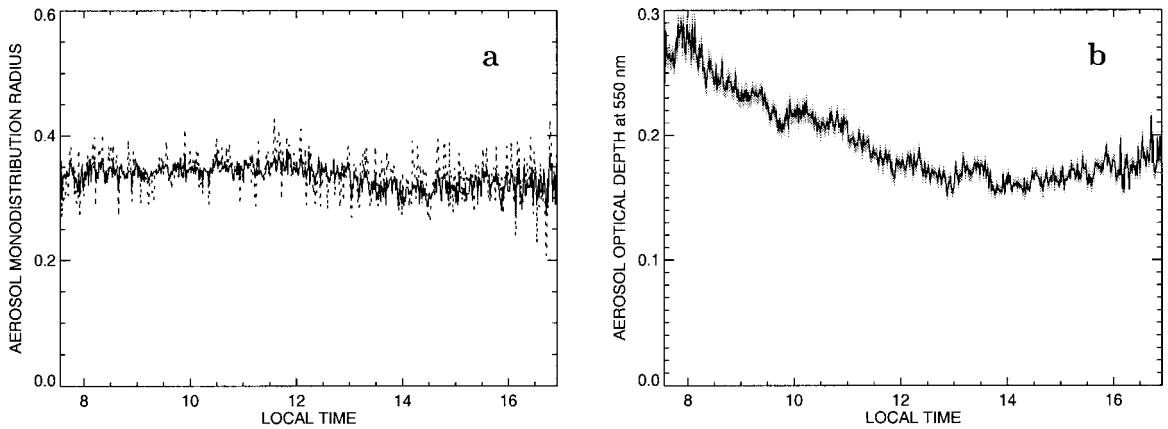

FIG. 6. (a) Time series of aerosol mean radius ($v_{\text{eff}} = 0$) for 2 Sep 1996, NYC: solid—from F_3, dashed—from F_4; (b) time series of aerosol optical depth in all five channels for the same day—the solid curve corresponds to $v_{\text{eff}} = 0.1$, the shaded area shows the effect of uncertainty in v_{eff} (between 0 and 0.4).

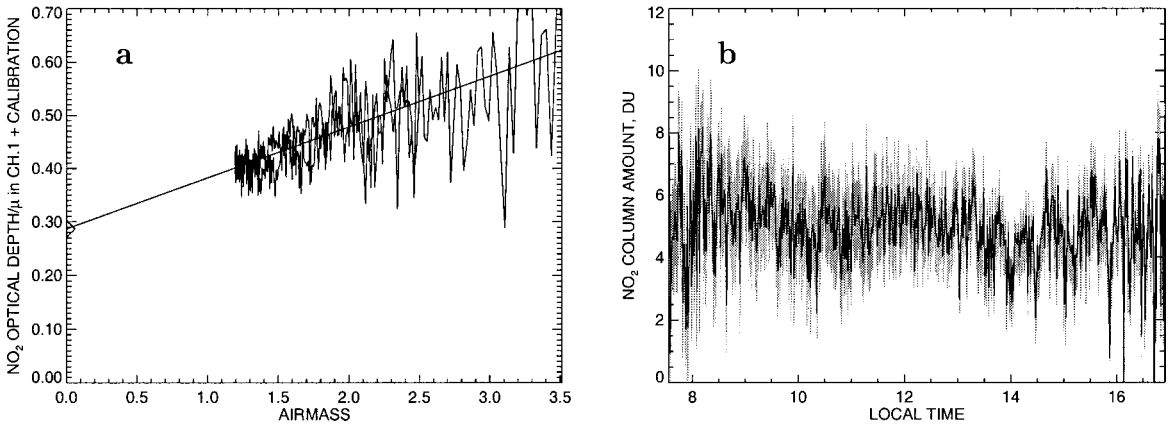

FIG. 7. (a) Regression plot for NO_2 optical depth in 415-nm channel (2 Sep 1996, NYC): diamond corresponds to the value of the calibration coefficient c_1 (here aerosol $\upsilon_{\text{eff}} = 0$ is assumed); (b) time series of NO_2 column amount (DU) for the same day: solid line corresponds to the assumed aerosol $\upsilon_{\text{eff}} = 0.1$, shaded region shows the uncertainty due to possible variation of υ_{eff} from 0 to 0.4.

Once the aerosol size has been determined the aerosol optical depth, at any wavelength, can be calculated from the Mie spectral extinction and the previously determined aerosol optical thickness in the 870-nm channel. Figure 6b shows the aerosol optical depth at 550 nm. In this particular case, it changes during the day violating the conditions for Langley analysis.

e. Retrieval of nitrogen dioxide column amounts

The aerosol optical depths calculated in the previous step are then subtracted from the observed total optical depths in all six channels. The remaining optical depth in the first channel (415 nm) is due to NO_2 absorption, while in the second channel (500 nm), both NO_2 and ozone absorption is present. Calibration uncertainties affect both channels, but NO_2 absorption is separated from calibration effects in the 415-nm channel by means of a Langley-like regression (Fig. 7a). The calibration coefficient c_1 is determined by this procedure together with the NO_2 column amount (Fig. 7b). We use Dobson units (1 DU $= 10^{-3}$ atm-cm $= 2.687 \times 10^{16}$ molecules cm^{-2}) to describe the NO_2 column amount as well as the ozone column amount.

Figures 7a and 7b show that urban [New York City (NYC)] nitrogen dioxide does not exhibit strong diurnal changes that are seen in stratospheric NO_2. Thus, the regression analysis is applicable; but unfortunately, this approach is not very accurate because of the strong interplay between the NO_2 column amount and the aerosol spectral extinction described above and the high variability of NO_2 in the urban New York environment. An uncertainty in the retrieved NO_2 column amount of 30%–50% is caused by our inability to uniquely constrain the variance υ_{eff} of the aerosol size distribution evident in Fig. 7b. On physical grounds, larger effective variances are likely to be more realistic than $\upsilon_{\text{eff}} = 0$. Also, neglect of aerosol absorption in the presence of absorbing aerosol also leads to some overestimation of the NO_2 column amount, while not significantly affecting the accuracy of other retrievals.

f. Retrieval of ozone column amounts

The standard approach to retrieve atmospheric ozone column amounts is to use the UV spectral region (Dobson and Brewer spectrometers). Nevertheless, the visible (Chappuis) absorption band has also been widely used to retrieve ozone column amounts (King and Byrne 1976; Shaw 1979a; Flittner et al. 1993; Michalsky et al. 1995). With aerosol removed, in our retrieval method the (uncalibrated) NO_2 absorption contributions are first analytically removed from the 500-nm channel measured optical depth. Then a Langley-like regression technique (Fig. 8a) is applied to obtain both the ozone column amount as function of time (Fig. 8b) and the calibration coefficient c_2. Here we emphasize that the retrieval of the ozone column amount has its own calibration procedure, making ozone retrievals almost independent of the retrievals of aerosol parameters and NO_2. If aerosol particle size does not dramatically change during the day (a condition met for most sites) then the contribution from errors in aerosol optical depth due to calibration errors has the form const. μ, which is corrected during the ozone calibration procedure. (The same is also true for errors in NO_2 calibration, even without any conditions on aerosol particle size.)

This procedure appears to be robust since the retrieved ozone column amount shows little change through the day. The small changes that are seen are mostly due to variations in surface ozone (Kerr and McElroy 1995). Despite large high-frequency variations due to instantaneous instrumental noise shown in Fig. 8b (the data have not been averaged), the mean ozone column amount is a well determined quantity, and column ozone can be retrieved with much better accuracy than NO_2. Moreover, by having filter channels on both the long- and short-wavelength sides of the ozone ab-

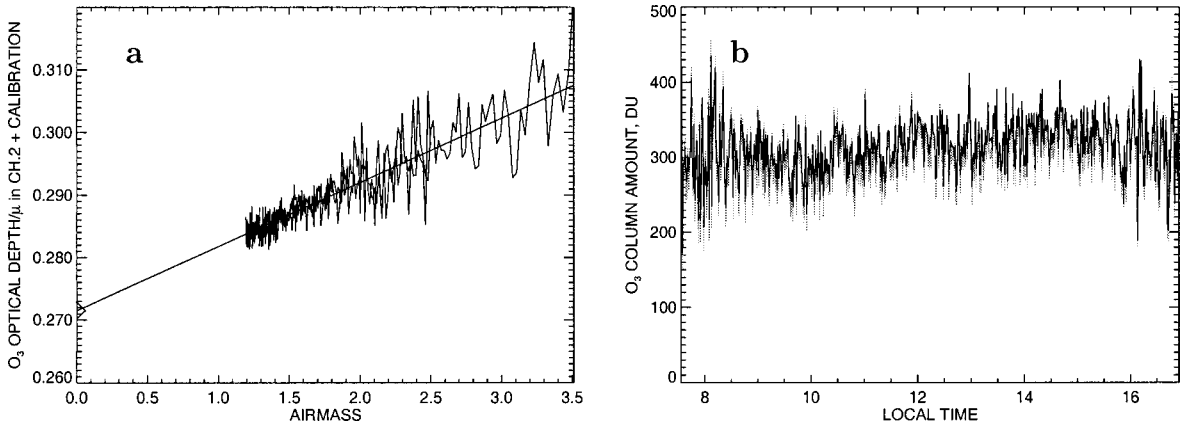

FIG. 8. (a) Regression plot for O_3 optical depth in 500-nm channel (2 Sep 1996, NYC): diamond corresponds to the value of the calibration coefficients combination $c_2 - b_{21}c_1$ (here aerosol $\upsilon_{\text{eff}} = 0$ is assumed); (b) time series of O_3 column amount (DU) for the same day: solid line corresponds to assumed aerosol $\upsilon_{\text{eff}} = 0.1$, the shaded area represents (small) uncertainty due to possible variation of υ_{eff} from 0 to 0.4.

sorption, it is possible to more effectively separate the ozone and aerosol contributions, unlike the situation for NO_2.

g. Calibration histories and calibration averaging

The method described in this paper provides for the simultaneous determination of the instrument's calibration together with the retrieval of physical quantities. In addition to the calibration coefficients determined in the previous steps, values of c_3 and c_4 can be obtained from A_3, A_4, c_1, and c_2, or directly by subtracting the retrieved optical depths from the measured ones. This information allows us to monitor any changes in the instrument's calibration.

The calibration history of the Goddard Institute for Space Studies (GISS) MFRSR during the period from 1 September 1995 to 27 November 1996 is shown in Fig. 9a (smoothed trends in Fig. 9b). The results show a loss of filter transmittance, approximately by a factor of 3 (assuming detector–electronics stability), for 615-nm and 670-nm channels during the first 200 days of operation, followed by a gradual stabilization. (This poor filter performance led to the replacement of these filters with ion assisted deposition filters in subsequent MFRSRs.) The transmission loss in the 415-nm and 500-nm channels was roughly 20% and 40%, respectively, while the 870-nm channel remained essentially stable. Subsequent laboratory recalibration of the instrument by the manufacturer (Yankee Environmental Systems, Inc.) confirmed these observed trends in filter transmittance. Since filter transmission can change rapidly (over the course of days), determining the calibration from the data on a daily basis allows us to catch these changes as they occur and correct them without compromising retrieval accuracy.

While our retrieval algorithm is designed to rely as little as possible on the values of the calibration coefficients, long-term smoothing allows us to improve the retrieval accuracy by reducing calibration noise that arises by including those days with short clear periods. Long-term smoothing of the calibration is reasonable since the instrument's calibration is not expected to vary significantly on a day-to-day basis. Some temperature-

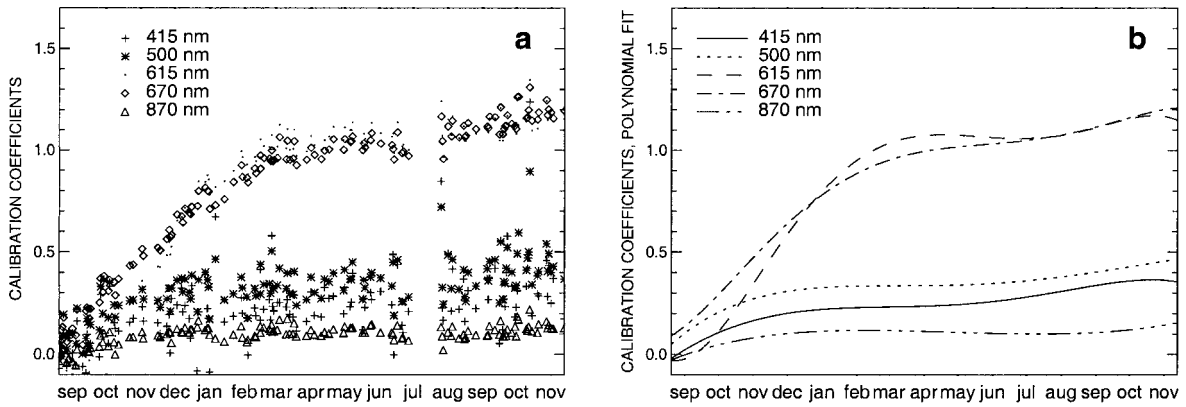

FIG. 9. Calibration history of the GISS MFRSR for the period from Sep 1995 to Nov 1996: (a) time dependence of calibration coefficients in five channels; (b) polynomial fits to the data from (a).

related fluctuations in filter transmission may occur, especially if the instrument head is not properly temperature stabilized. However, based on our comparisons with other measurements [e.g., CIMEL Total Ozone Mapping Spectrometer (TOMS), Brewer spectrometer] we have found that most day-to-day variations in the instantaneous MFRSR calibrations derived from the data are correlated with differences in the retrieval products. This suggests that the variability in the instantaneous calibration coefficients is attributable to uncertainties in the calibration technique, rather than actual instrumental effects, in particular, effects due to changes in the diffuse horizontal measurement due to clouds outside the MFRSR field of view on partially cloudy days.

To control for these situations, the data are reprocessed using smooth approximations of the calibration time series. Figure 9b shows such approximations (made by 5 degree polynomial fits) of the calibration coefficients from Fig. 9a. The method used to average the calibration coefficients must preserve the spectral dependence of the measured optical depths. Otherwise, the averaging will affect the retrievals that rely on spectral differences in optical depths (such as particle size and ozone).

To achieve spectral consistency, we perform calibration averaging and data reprocessing using a procedure that follows the steps of the instantaneous retrieval algorithm. This averaging–reprocessing procedure requires that we repeat the retrievals four times for all days during the selected data period. On the first step, we smooth the 870-nm calibration coefficient c_5 over the time period. Then we rerun the retrievals with the smoothed c_5 to obtain the adjusted values of A_3. These values are then also smoothed over the selected time period, and the retrievals are repeated providing corrections to the value of c_1 that is determined from the calibration of the NO_2 column amount. Next, we reprocess the data (with smoothed values of c_5, A_3, and c_1) to produce adjusted ozone calibration coefficients that are then smoothed before the final reprocessing is performed.

We note that the results of reprocessing, with smoothed calibration coefficients depend on the specific method of smoothing. This dependence is most pronounced for the ozone retrievals. Since we prefer a technique that is less sensitive to the algorithmic details, we apply a weighted average of the instantaneous and smoothed ozone calibration coefficients where the weighting factors are determined from the quality of the instantaneous regression plot.

3. Comparison with other methods and measurements

a. Comparison with instantaneous Langley regressions

We compared our retrieved calibration coefficients and optical depths with those determined by Langley regressions using a particularly clear dataset obtained from the U.S. Department of Agriculture (USDA) ultraviolet B (UVB) Radiation Program (Bigelow et al. 1998) for Davis, California (January–July 1996). Only completely cloud-free days are used in this comparison (Alexandrov et al. 1999b). Comparison between the calibration coefficients for the 870-nm channel derived using our direct–diffuse technique and those determined from Langley regression are shown in Fig. 10a. Both approaches yield similar calibration coefficients and follow the same general trend, but, the instantaneous calibration coefficients determined using our direct–diffuse technique show less variability (due in part to a better agreement between the morning and afternoon regressions) and are therefore more stable. The results of comparisons for the other channels are similar, with the exception of the first channel (415 nm) where the advantages of the direct–diffuse approach are less pronounced due to variations in the NO_2 column amount.

The overall difference between the instantaneous daily mean optical depths obtained by the two methods is relatively small as shown in Fig. 10b. Differences are typically less than 0.01 and do not exceed 0.04 during this period. Since optical depth differences of 0.04 are larger than would be expected from well-calibrated data, we performed additional comparisons. Figure 11 compares the Langley regression to our method for a day (2 June 1996) with good agreement. As can be seen, when both methods are applicable, they yield the same result. However, on two other days, shown in Fig. 12, we see that our method produces stable regressions while the Langley method yields morning and afternoon differences that would most likely exclude the data for 9 May shown in Fig. 12a from further analysis, while Langley analysis of the data for 8 June shown in Fig. 12b converges to yield a calibration coefficient not very different from our result. Thus, our regression algorithm provides an objective test of the accuracy of the Langley regression and allows us to retrieve aerosol and gas column amounts from data that would have otherwise have to be excluded.

b. Comparison with AERONET optical depth retrievals

We also compared our calibrations and optical depth retrievals with the optical depths derived from measurements by the Aerosol Robotic Network (AERONET; Holben et al. 1998) CIMEL sun–sky radiometer collocated with MFRSR at the Atmospheric Radiation Measurement (ARM) Cloud and Radiation Testbed (CART) site central facility. Level 2.0 AERONET data are used. These measurements have been cloud-screened and quality-controlled according to Smirnov et al. (2000). We sampled the MFRSR data to match the measurement times of the CIMEL measurements (they are less frequent in time) and selected for this comparison data collected during the period from January to June

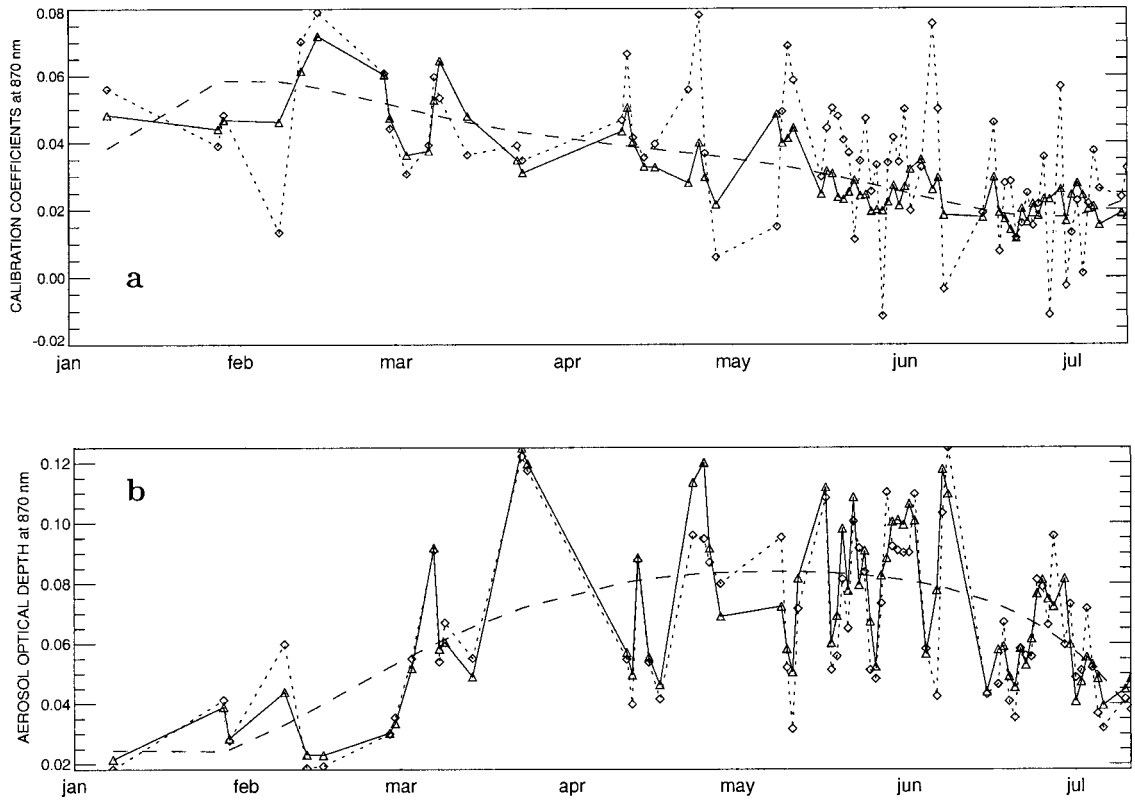

FIG. 10. Comparison between the results obtained on the Davis, CA 1996 dataset by the proposed method (solid lines) and the Langley method (dotted lines); dashed line represents polynomial fit: (a) calibration coefficients, (b) aerosol optical depths at 870 nm.

1999. During this time period there were 58 clear or partially clear days with data available from both instruments (total 1342 data points). This period contains a variety of atmospheric conditions with aerosol optical depths ranging from 0.03 to 0.4 (at 500-nm wavelength). The MFRSR calibrations and retrievals are performed according to the algorithm described in this paper, including smoothing of the calibration coefficients.

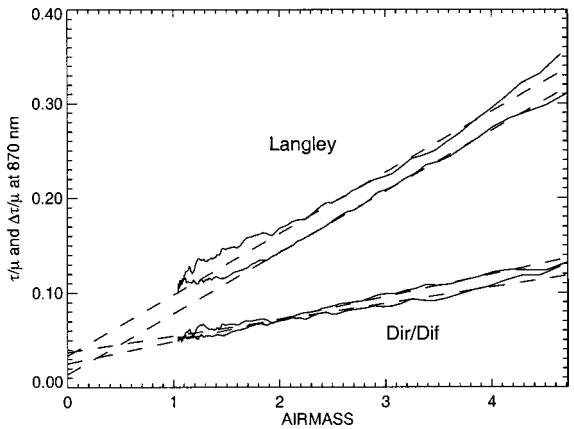

FIG. 11. Comparison between the Langley regression plots and the regression plots of the differences between optical depths derived from direct beam measurements and from direct-to-diffuse ratios for Davis, CA, 2 Jun 1996. Intersection of the dashed lines with the vertical axis corresponds to the value of the calibration coefficient c_5 (obtained in the morning or afternoon).

The 500-, 670-, and 870-nm channels are common to both the CIMEL and MFRSR. For comparison with the 440-nm CIMEL channel, we interpolated between our retrieved optical depths at 415 and 500 nm to obtain an MFRSR-derived estimate of the optical depths at 440 nm.

The AERONET retrieval algorithm neglects the contribution of NO_2 absorption to the retrieved optical depths. Therefore, in this comparison, we have added the NO_2 optical depths to our aerosol optical depths; that is, the comparison is between the total optical depths measured by the two instruments with ozone contribution subtracted. Differences between the climatological ozone column amounts (used by AERONET) and the values retrieved using our algorithm, appear to have a negligible effect on this comparison.

Figure 13 presents scatterplots comparing MFRSR and CIMEL optical depths at 440-, 500-, 670-, and 870-nm wavelengths. Mean differences between our MFRSR retrievals and the AERONET ones do not exceed 0.005 for 440-, 500-, and 870-nm channels with standard deviation of 0.01 or less for all channels. This agreement is similar to that obtained by Halthore et al. (1997) who compared MFRSR- and CIMEL-derived optical depths at the same site for April 1994 (where the agreement

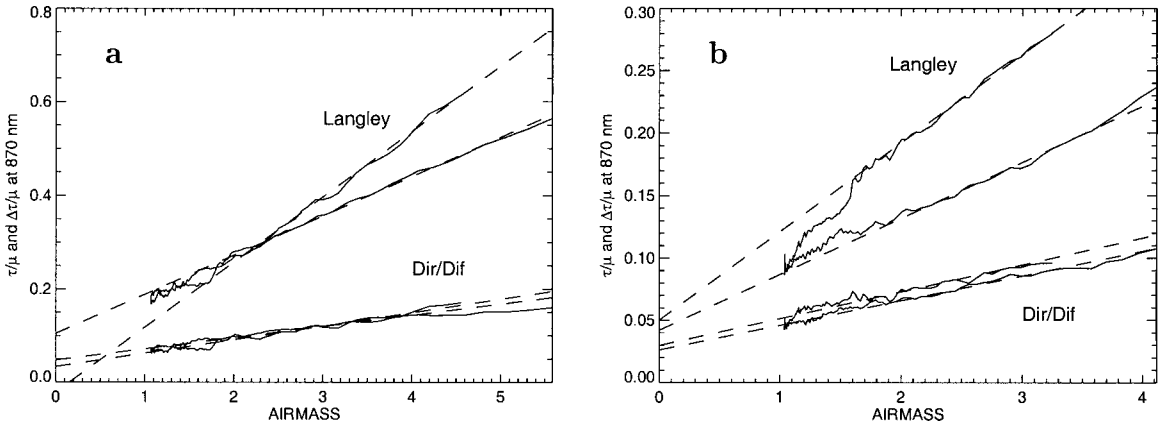

FIG. 12. Same as in Fig. 11 but for (a) 9 May and (b) 8 Jun 1996.

was within ±0.01) and April 1996 (where the agreement was within ±0.02). Similarly, Schmid et al. (1999) found that CIMEL–MFRSR differences do not exceed 0.01 for all wavelengths on 29 September and 2 October 1997 using collocated measurements at the Southern Great Plains (SGP) Central Facility. The MFRSR calibration in both of these studies is based on the robust estimate made using the 20 nearest successful Langley plots. While the CIMEL calibration is based on periodic high altitude Langley recalibrations.

We find that small systematic differences exist for the 670-nm channel. Here the MFRSR optical depths are biased compared with those derived from the CIMEL by 0.01. This bias, while not exceeding the commonly accepted calibration accuracy, reflects a difference in spectral slopes between 670- and 870-nm optical depths measured by these two instruments. The aerosol optical depths are expected to monotonically decrease with increasing wavelength in this spectral region (note that NO_2 absorption does not influence this behavior: it is absent at 870 nm and is only about 10^{-4} per DU at 670 nm). This behavior is observed in all MFRSR retrievals and in the most of the CIMEL results. However, the CIMEL-determined slope between the two channels is systematically smaller. The difference is more pronounced during winter when the aerosol particles are larger and therefore generally exhibit smaller spectral slopes. On some days, the CIMEL-determined slope becomes negative, which while possible, in these particular cases seems to be inconsistent with spectral behavior of optical depths at other wavelengths. For these days, the CIMEL-derived aerosol optical depth at 670 nm is smaller than that at 870 nm and sometimes even smaller than that determined at 1020 nm. Further, we note that the original (level 1.0) AERONET data for these days are spectrally monotonic, while exhibiting certain calibration artifacts. Calibration changes made in level 2.0 processing might be responsible for these differences. While our algorithm precludes a behavior that is inconsistent with Mie theory, the residuals in our retrieval of the 670-nm optical depths are typically of order 10^{-4} and do not exceed 10^{-3} for the dataset considered. Thus, our residuals cannot explain the observed bias.

c. *Validation of nitrogen dioxide retrievals: Comparison with Brewer spectrometer data*

Our MFRSR-retrieved ozone and NO_2 column amounts are compared with those derived from Brewer spectrophotometer measurements. The Brewer data are taken from Environmental Protection Agency (EPA) UV Monitoring Program (http://www.epa.gov/uvnet/) site at Big Bend National Park, Texas. This site is located at 29.305° latitude and 103.177° longitude, and the site elevation is 1052 m above sea level. The nearest MFRSR site belongs to the USDA UVB Radiation Program and is about 35 km southwest (29.133° latitude and 103.517° longitude) and at a lower altitude (670 m). Because the two instruments are not exactly collocated, precise agreement is not expected since polluted air masses of the same origin may reach the two sites at different times and, due to transport processes, may have different concentrations. Since, ozone is mostly stratospheric, its measurements are not affected significantly by local atmospheric transport, and better agreement between the instruments should be observed.

The period from February to May 1999 with good quality data available from both instruments was selected for this comparison. Brewer retrievals are made from direct sun measurements. Figure 14 shows the Brewer-retrieved (diamonds with error bars) and MFRSR-retrieved (shaded rectangles) NO_2 column amounts for this period. The mean difference between the minimal and maximal limits of the MFRSR NO_2 retrievals is 3 DU. Most of the Brewer points have uncertainties of about ±0.5 DU. As can be seen, most of the retrieved NO_2 column amounts agree within these uncertainties.

The NO_2 column amounts derived from both the MFRSR and Brewer data are generally considered to be too high for a national park; however, it is likely that

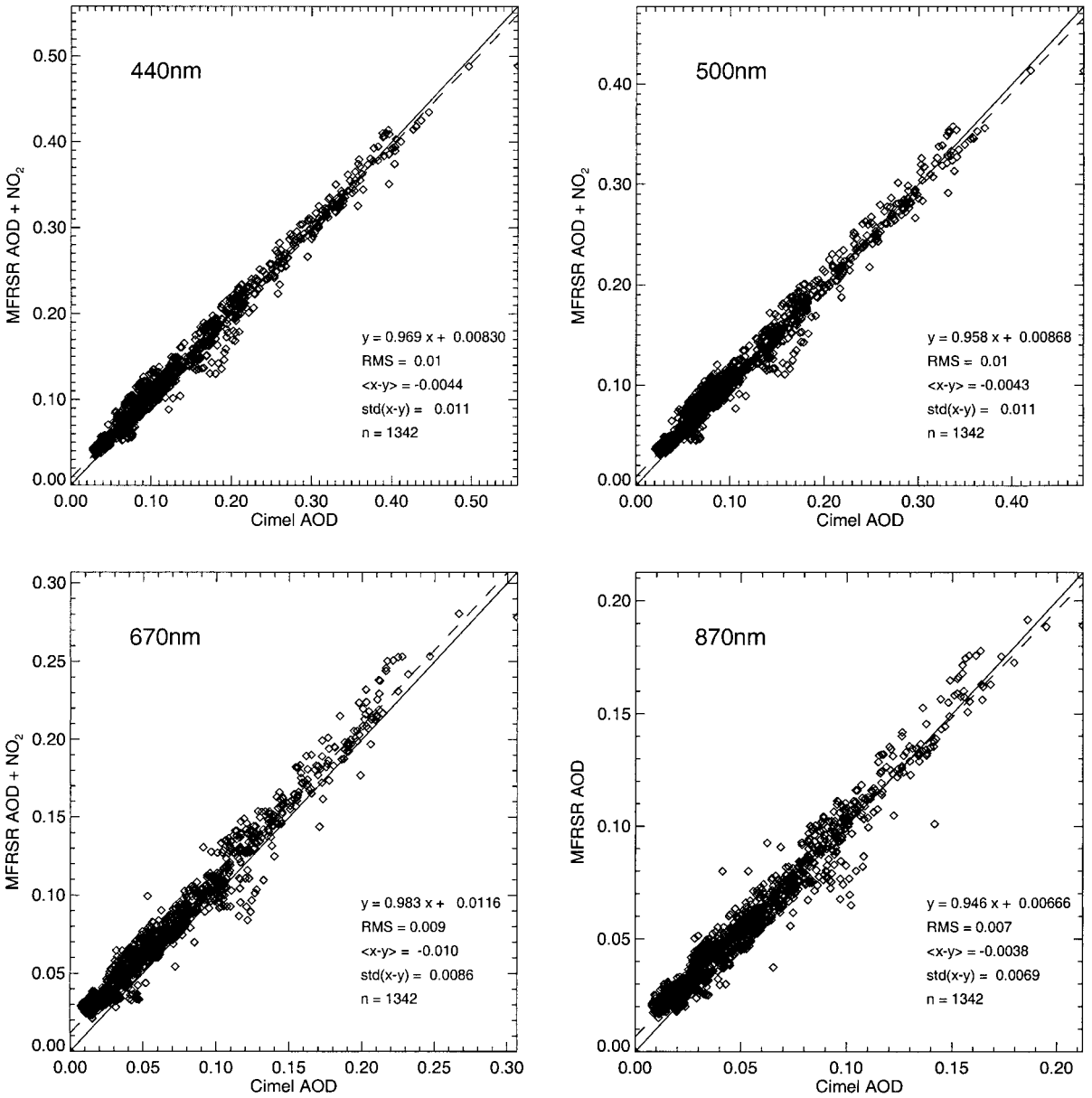

FIG. 13. Comparison between optical depth retrievals from MFRSR data according to the described algorithm and these from collocated CIMEL sun photometer (AERONET level 2.0 data). The data was obtained at DOE ARM Program CART site central facility during the period from Jan to Jun 1999 (58 clear days).

they can be attributed to air quality problems at this particular location. According to the National Parks Service (http://www.nps.gov/bibe/aqvis.htm), the air quality in the Big Bend National Park experienced noticeable changes during the 1970s. The air monitoring program, begun in 1978, has allowed park managers to interpret the transport and transformation of pollutants that contribute to air quality problems within their park. Among the major sources that contribute to Big Bend's pollution are North–Central Mexico, including the urban and industrial region of Monterrey and Monclova; East–Central Texas and the Gulf Coast, including the urban and industrial areas of Houston and Galveston; and Mexico City and its surrounding urban area. There are no high-ground concentrations of NO_2 measured within the park since pollutants that are transported to the park from remote sources are likely to be concentrated at a higher altitude.

d. Validation of ozone retrievals: Comparison with Brewer and TOMS data

Figure 15 presents the comparison between the MFRSR-derived ozone column amounts and those de-

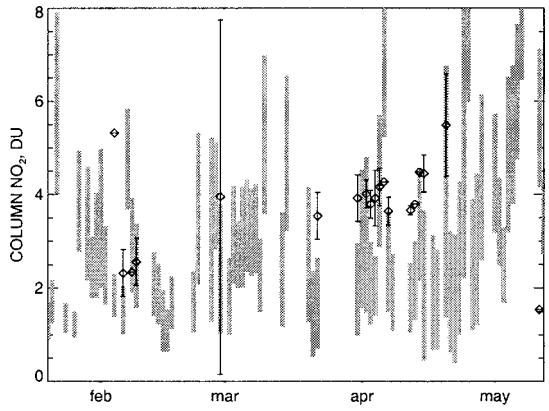

FIG. 14. Comparison between daily mean NO_2 column amounts retrieved from MFRSR data according to the described algorithm (shaded boxes) and these from the EPA UV-net Brewer spectrometer (diamonds) located at 35 km NE from the MFRSR site. The data was obtained at Big Bend National Park, TX, during the period from Feb to May 1999 (74 MFRSR daily values, 22 Brewer daily values).

rived from Brewer (20 data points) and TOMS (70 data points) measurements as well as a comparison between the Brewer- and TOMS-derived ozone column amounts (21 data points; the TOMS values are referenced to the MFRSR site). The MFRSR ozone retrievals appear to be practically unbiased when compared with the TOMS values (the mean difference is -0.35 DU, i.e., about 0.1% of a typical ozone column amount). The standard deviation is 18 DU and may represent both uncertainties of the measurements and difference in averaging/sampling between satellite- and ground-based measurements. The Brewer retrievals (provide fewer data points for comparison) show some 7–10 DU bias (overestimation) compared to both MFRSR and TOMS with the standard deviation of the same order (14–20 DU) as for the MFRSR–TOMS comparison.

Previously comparisons with EPA Brewer-derived ozone column values and those obtained from shadowband radiometer measurements (in UV) were performed by Slusser et al. (1999) who found that the ultraviolet rotating shadowband radiometer-retrieved ozone column amounts overestimate those derived from the Brewer measurements by 1% (3 DU, relative to the typical value of 300 DU) on average with standard deviation of 2% (6 DU). This accuracy is better than what we obtain with the visible MFRSR, which is to be expected based on the strength of the ozone absorption in the UV. Comparisons between TOMS ozone retrievals and those obtained from direct sun measurements at 29 Brewer stations worldwide were reported by Fioletov et al. (1999). They found results that vary with location with biases ranging from 0.1% to 6.6% (corresponding to 0.3–20 DU) and standard deviations ranging from 0.9% to 5.2% (3–15 DU). Kerr and McElroy (1995) report 4.6% (13.7 DU) bias with TOMS for their direct sun measurements at Table Mountain Observatory. In our case the differences are of the same order: 10 DU bias and 14.4 DU standard deviation.

Figures 16–18 present the comparison of MFRSR-derived ozone column amounts with TOMS measurements for three additional sites: Albany, New York, [Atmospheric Sciences Research Center (ASRC)], New York City (GISS), and Department of Energy (DOE) ARM CART site central facility (Southern Great Plains, Oklahoma). For the latter site, we use the same data previously used in our comparison with the AERONET optical depth measurements described above. All three plots show data from periods containing 40–60 clear days. As described above, the calibration smoothing procedure has been applied to all of these datasets. Calibration smoothing results in a reduction of the standard deviation of the differences by up to 30% when compared with the instantaneous retrievals. The accuracy of MFRSR ozone retrievals depends on both the atmospheric conditions at the instrument location and probably on some instrumental characteristics. We have found that some MFRSRs tend to systematically underestimate the column ozone amounts (compared to TOMS). Among these three datasets, the Albany instrument shows the largest bias (29 DU) when compared with TOMS measurements. The other two instruments exhibit smaller biases that are comparable to those observed in Brewer and Dobson spectrometer comparison (Fioletov et al. 1999), while the standard deviations in MFRSR comparisons with TOMS are generally larger than those for the spectrometric measurements.

4. Discussion

We have described a retrieval algorithm for processing MFRSR data that allows derivation of time series of aerosol optical depth and effective particle size, as well as of ozone and NO_2 column amounts. This algorithm also provides calibration coefficients for the instrument, so that laboratory pre- and postcalibration is unnecessary. This method is designed in such a way that calibration errors in the determination of one parameter (e.g., aerosol optical depth) do not significantly affect the accuracy of other retrievals (e.g., of aerosol particle size or gas column amounts) and the determination of the calibration is coupled with the retrieval.

As a calibration method, our approach is applicable to wider range of atmospheric conditions than the traditional Langley technique. This allows us to include more data in the analysis than would be possible if we had to rely solely on the Langley approach. The initial calibration of 870-nm channel is performed by comparison of direct beam optical depth with that retrieved from direct to diffuse ratio. By adopting this approach, we are able to maximize the number of days (or time periods) that we can include in our analysis. Moreover, as shown, this method does not require exceptional stability of the atmosphere.

While we have not yet fully utilized the information

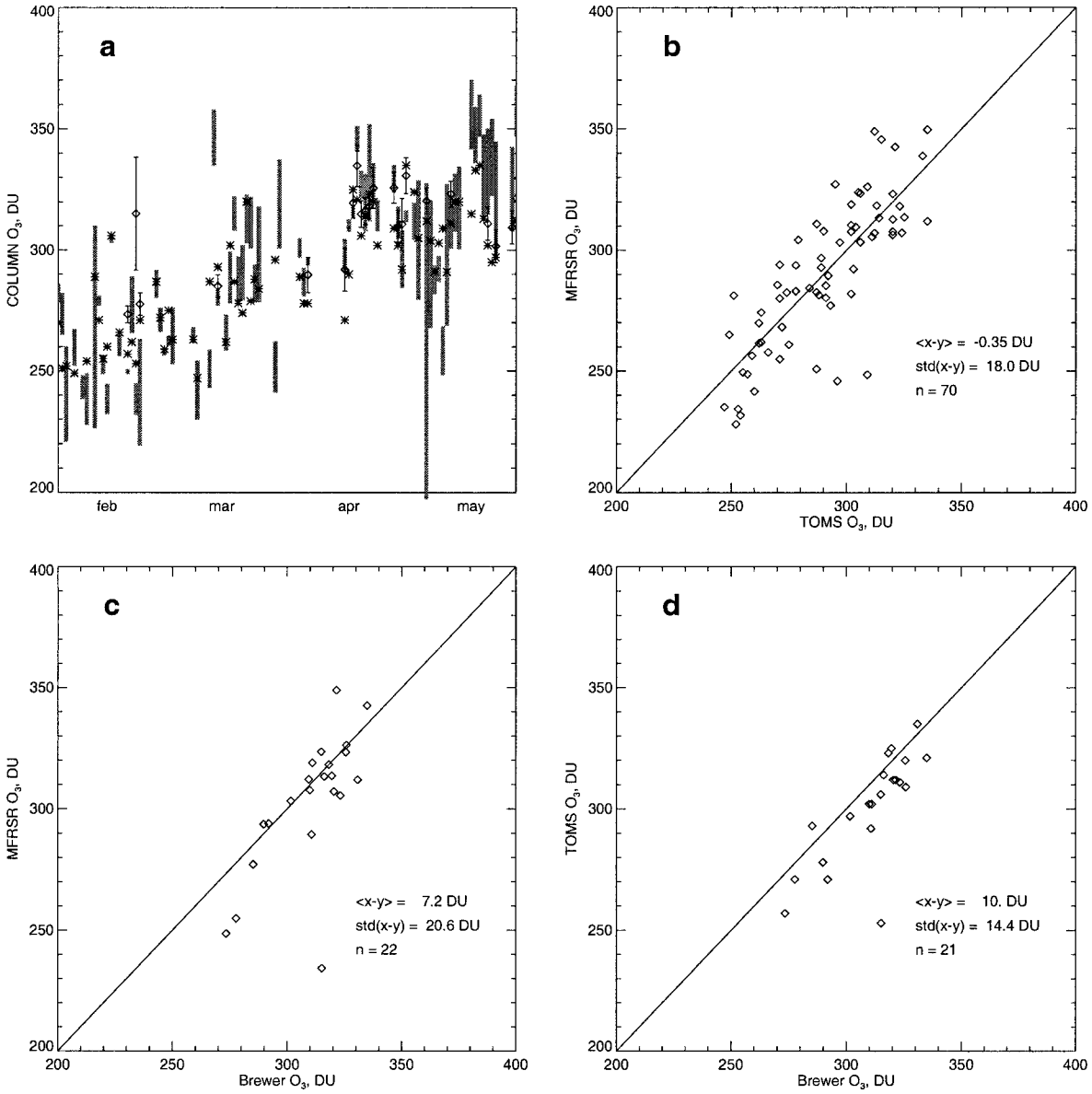

FIG. 15. (a) Comparison between daily mean ozone column amounts retrieved from MFRSR data according to the described algorithm (shaded boxes), these from the EPA UV-net Brewer spectrometer (diamonds), and TOMS satellite measurements over the MFRSR site. The data was obtained at Big Bend National Park, TX, during the period from Feb to May 1999 (74 MFRSR daily values, 22 Brewer daily values, 70 TOMS values). (b)–(d) Scatterplots comparing retrievals by each pair of the instruments: (b) MFRSR–TOMS, (c) MFRSR–Brewer, (d) TOMS–Brewer.

content of the MFRSR measurements since we are only using the diffuse measurements at 870 nm, we have developed an algorithm that self-consistently retrieves both aerosol properties and gas column amounts from the measurements. We have shown that our method provides results that are comparable to those obtained using the traditional Langley technique but exhibit greater stability.

Comparison of our MFRSR-derived ozone column amounts with TOMS ozone retrievals shows that the bias and standard deviation is similar to that reported for Brewer–TOMS comparisons, although there are indications that the accuracy of the ozone retrieval from UV measurements is higher than that from these visible measurements. Moreover, we have found that the accuracy of our ozone retrievals depends on specific characteristics of the individual MFRSRs suggesting that it should be possible to increase the accuracy of these retrievals through a better understanding of these instrumental differences.

At present, it is difficult to validate the accuracy of our NO_2 retrievals due to the paucity of correlative mea-

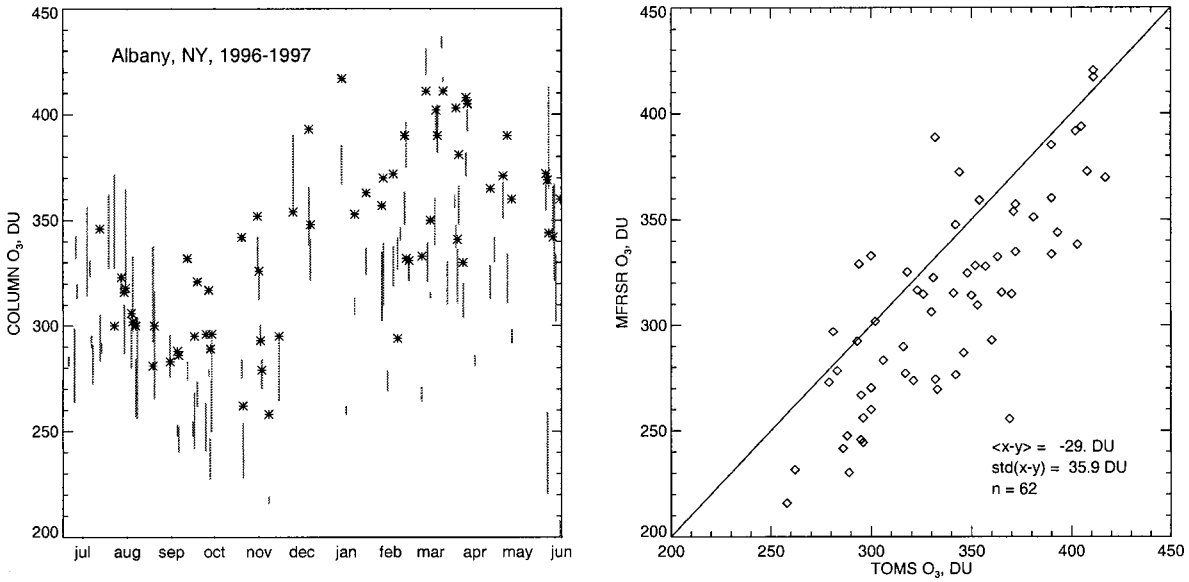

FIG. 16. Comparison between MFRSR ozone retrievals and TOMS satellite measurements for Albany, New York (ASRC), Jul 1996–Jun 1997. Left: time series of daily ozone values (MFRSR values with uncertainties are depicted by shaded boxes, TOMS values by stars). Right: scatterplot comparison for the same period (here aerosol $\upsilon_{\text{eff}} = 0.2$ is assumed).

surements. Nonetheless, comparison between nearby MFRSR and Brewer spectrometer measurements show generally good agreement given the relatively large uncertainty in our NO_2 retrieval due to our inability to constrain the aerosol size distribution. Shaw (1976) suggested that neglect of NO_2 absorption can lead to significant errors in aerosol optical depth. The magnitude of the errors was quantified by Schroeder and Davies (1987) who analyzed concurrent measurements of spectral direct beam solar radiation and column NO_2 at a suburban site in Hamilton, Ontario. Using a differential absorption spectrometer to measure NO_2 column amounts, they found values ranging from near 0.04 to 12 DU with a median of 1.7 DU, that is within the range of other published values (Noxon 1978; Pujadas et al. 2000). Moreover, they found that inclusion of NO_2 absorption significantly reduced the aerosol optical depths, decreased the retrieved aerosol number density and mass. Finally, at high NO_2 amounts, they found that the inclusion of NO_2 absorption narrowed the size distribution derived from median optical depths and changed it from bimodal to unimodal.

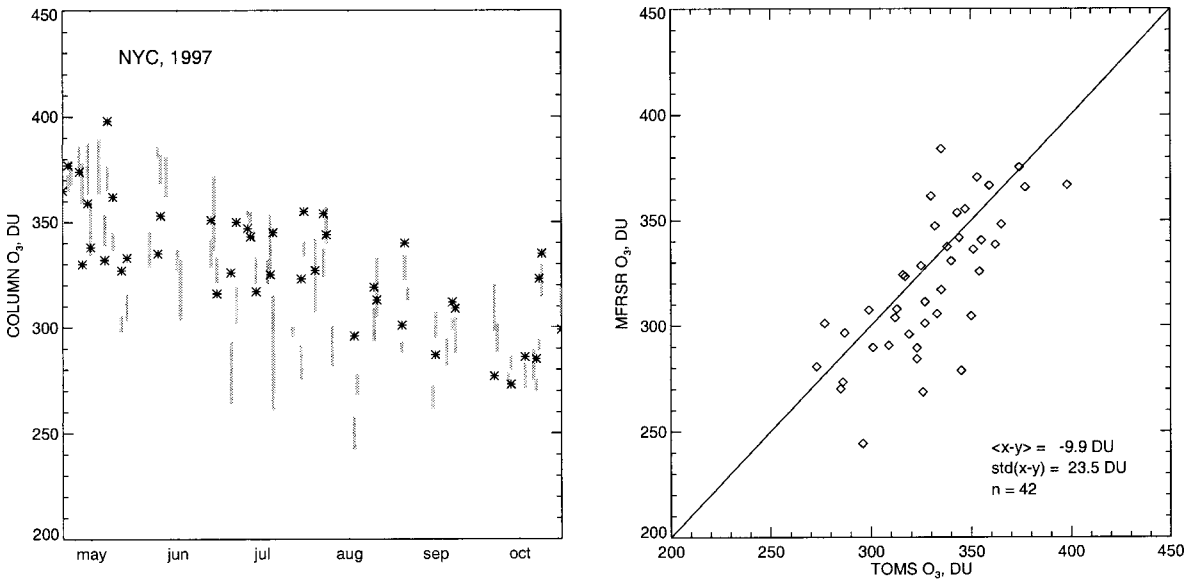

FIG. 17. The same as Fig. 16, but for New York City (GISS), May–Oct 1997.

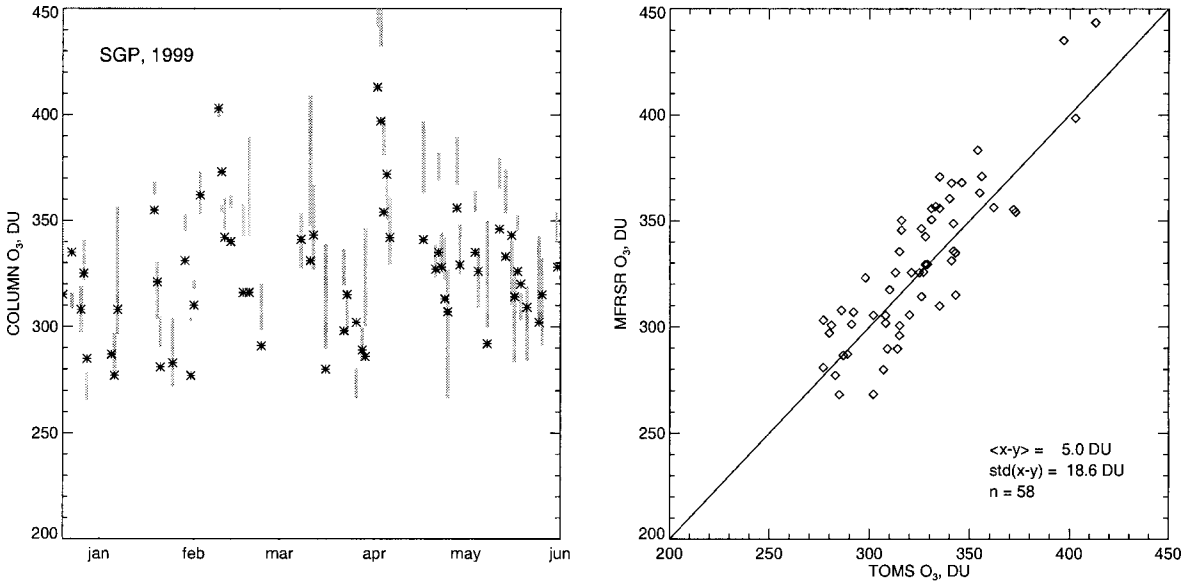

FIG. 18. The same as Fig. 16, but for Southern Great Plains, OK (DOE ARM CART), Jan–Jun 1999.

Leue et al. (2001) report GOME level-2 tropospheric NO_2 residuals exceeding 2.0×10^{15} molecules cm^{-2} in the metropolitan New York area. While our values are considerably larger than these tropospheric residuals, it is likely that the current GOME level-2 values underestimate tropospheric NO_2 because of an overestimate of the ground albedo in the blue spectral range and the deviation of the real atmosphere from the monthly and seasonal air mass factors used in the processing (Leue et al. 2001). Moreover, the effects of subpixel clouds and spatial averaging of high and low NO_2 tropospheric amounts within the GOME field of view would further reduce the GOME values relative to ground-based retrievals (Thomas et al. 1998). Nonetheless, the GOME measurements show strongly enhanced NO_2 columns over industrialized areas as well as regions of intense biomass burning with tropospheric NO_2 values varying by at least an order of magnitude between unpolluted oceanic and polluted urban areas. Thus, our results, combined with GOME measurements, reveal that the tropospheric amount of NO_2 is highly variable in both space and time.

Since we would like to improve the accuracy of our NO_2 retrieval and simultaneously better constrain the aerosol size distribution, we will be exploring ways to more fully exploit the information content of the MFRSR measurements through a more complete analysis of the diffuse flux measurements. Moreover, it is likely that these measurements augmented with measurements at higher spectral resolution over a broader spectral interval such as those made with the rotating shadowband spectroradiometer (Harrison et al. 1999) will provide a more complete description of aerosol properties and a more accurate NO_2 column amount.

This algorithm is being used to analyze data from a variety of different MFRSRs under a variety of atmospheric and surface conditions to more fully test the performance of the algorithm. These results are presented in our companion paper (Alexandrov et al. 2002) along with a discussion of the seasonal and geographic variation in aerosol and the use of MFRSR data in constructing aerosol climatologies.

Acknowledgments. We would like to thank M. Mishchenko for providing the Mie scattering code and for useful discussions; J. Michalsky for technical information on MFRSRs from ASRC network; the DOE ARM Program, AERONET, and R. Halthore for CIMEL data from SGP site; D. Shindell for information about NO_2 photochemistry; and posthumously thank D. Bigelow for providing data from the USDA UVB network. We are indebted to the three reviewers of this paper, their detailed comments improved this manuscript. This work was supported by NASA's Radiation Science Program and the Department of Energy Atmospheric Radiation Measurement Program.

REFERENCES

Alexandrov, M., A. Lacis, B. Carlson, and B. Cairns, 1999a: Remote sensing of atmospheric aerosols, nitrogen dioxide and ozone by means of multi-filter rotating shadow-band radiometer. *Proc. SPIE,* **3867,** 156–170.

——, ——, ——, and ——, 1999b: Validation of MFRSR data analysis: Comparison with the Langley approach. *Proc. Ninth Annual Atmospheric Radiation Measurement (ARM) Program Science Team Meeting,* San Antonio, TX, Department of Energy, [Available online from http://www.arm.gov/docs/documents/technical/conf_9903.]

——, ——, ——, and ——, 2002: Remote sensing of atmospheric aerosols and trace gases by means of multifilter rotating sha-

dowband radiometer. Part II: Climatological applications. *J. Atmos. Sci.,* **59,** 544–566.
Anderson, S. M., and K. Mauersberger, 1992: Laser measurements of ozone absorption cross sections in the Chappuis band. *Geophys. Res. Lett.,* **19,** 933–936.
Bigelow, D. S., J. R. Slusser, A. F. Beaubien, and J. H. Gibson, 1998: The USDA Ultraviolet Radiation Monitoring Program. *Bull. Amer. Meteor. Soc.,* **79,** 601–615.
Bodhaine, B. A., N. B. Wood, E. G. Dutton, and J. R. Slusser, 1999: On Rayleigh optical depth calculations. *J. Atmos. Oceanic Technol.,* **16,** 1854–1861.
Burkholder, J. B., and R. K. Talukdar, 1994: Temperature dependence of the ozone absorption spectrum over the wavelength range 410 to 760 nm. *Geophys. Res. Lett.,* **21,** 581–584.
Burrows, J. P., A. Dehn, B. Deters, S. Himmelmann, A. Richter, S. Voigt, and J. Orphal, 1998: Atmospheric remote-sensing reference data from GOME-1. Temperature dependent absorption cross sections of NO_2 in the 231–794-nm range. *J. Quant. Spectrosc. Radiat. Transfer,* **60,** 1025–1031.
——, A. Richter, A. Dehn, B. Deters, S. Himmelmann, S. Voigt, and J. Orphal, 1999: Atmospheric remote-sensing reference data from GOME-2. Temperature dependent absorption cross sections of O_3 in the 231–794-nm range. *J. Quant. Spectrosc. Radiat. Transfer,* **61,** 509–517.
Charlson, R. J., S. E. Schwartz, J. M. Hales, R. D. Cess, J. A. Coakley, J. E. Hansen, and D. J. Hofmann, 1992: Climate forcing be atmospheric aerosols. *Science,* **255,** 423–430.
Dubovik, O., and M. D. King, 2000: A flexible inversion algorithm for retrieval of aerosol optical properties from Sun and sky radiance measurements. *J. Geophys. Res.,* **105,** 20 673–20 696.
Fioletov, V. E., J. B. Kerr, E. W. Hare, G. J. Labow, and R. D. McPeters, 1999: An assessment of the world ground-based total ozone network performance from the comparison with satellite data. *J. Geophys. Res.,* **104,** 1737–1747.
Flittner, D. E., B. M. Herman, K. J. Thome, J. M. Simpson, and J. A. Reagan, 1993: Total ozone and aerosol optical depths inferred from radiometric measurements in the Chappuis absorption band. *J. Atmos. Sci.,* **50,** 1113–1121.
Forgan, B. W., 1994: General method for calibrating Sun photometers. *Appl. Opt.,* **33,** 4841–4850.
Halthore, R. N., and S. E. Schwartz, 2000: Comparison between model-estimated and measured diffuse downward irradiance at surface in cloud-free skies. *J. Geophys. Res.,* **105,** 20 165–20 177.
——, ——, J. J. Michalsky, G. P. Anderson, R. A. Ferrare, B. N. Holben, and H. M. ten Brink, 1997: Comparison of model estimated and measured direct-normal solar irradiance. *J. Geophys. Res.,* **102,** 29 991–30 002.
——, S. Nemesure, S. E. Schwartz, D. G. Imre, A. Berk, E. G. Dutton, and M. H. Bergin, 1998: Models overestimate diffuse clear-sky surface irradiance: A case for excess atmospheric absorption. *Geophys. Lett.,* **25,** 3591–3594.
Hansen, J. E., and L. D. Travis, 1974: Light scattering in planetary atmospheres, *Space Sci. Rev.,* **16,** 257–610.
——, and Coauthors, 1995: Low-cost long-term monitoring of global climate forcing and feedbacks. *Climatic Change,* **31,** 246–271.
——, M. Sato, A. Lacis, and R. Ruedy, 1997: The missing climate forcing. *Philos. Trans. Roy. Soc. London,* **352B,** 231–240.
——, ——, R. Ruedy, A. Lacis, and V. Oinas, 2000: Global warming in the twenty-first century: An alternative scenario. *Proc. Natl. Acad. Sci.,* **97,** 9875–9880.
Harrison, L., and J. Michalsky, 1994: Objective algorithms for the retrieval of optical depths from ground-based measurements. *Appl. Opt.,* **33,** 5126–5132.
——, ——, and J. Berndt, 1994: Automated multifilter shadow-band radiometer: instrument for optical depth and radiation measurement. *Appl. Opt.,* **33,** 5118–5125.
——, M. Beauharnois, J. Berndt, P. J. Kiedron, J. Michalsky, and Q. L. Min, 1999: The rotating shadowband spectroradiometer (RSS) at SGP. *Geophys. Res. Lett.,* **26,** 1715–1718.
Herman, B. M., R. S. Browning, and J. J. De Luisi, 1975: Determination of the effective imaginary term of the complex refractive index of atmospheric dust by remote sensing: The diffuse-direct radiation method. *J. Atmos. Sci.,* **32,** 918–925.
Holben, B. N., and Coauthors, 1998: AERONET—A federated instrument network and data archive for aerosol characterization. *Remote Sens. Environ.,* **66,** 1–16.
Kato, S., T. P. Ackerman, E. E. Clothiaux, J. H. Mather, G. G. Mace, M. L. Wesely, F. Murcray, and J. Michalsky, 1997: Uncertainties in modeled and measured clear-sky surface shortwave irradiances. *J. Geophys. Res.,* **102,** 25 881–25 898.
Kerr, J. B., and C. T. McElroy, 1995: Total ozone measurements made with the Brewer ozone spectrophotometer during STOIC 1989. *J. Geophys. Res.,* **100,** 9225–9230.
Kiehl, J. T., and H. Rodhe, 1995: Modeling geographical and seasonal forcing due to aerosols. *Aerosol Forcing of Climate,* R. J. Chaarlson and J. Heintzenberg, Eds., J. Wiley, 281–296.
King, M. D., 1979: Determination of the ground albedo and the index of absorption of atmospheric particulates by remote sensing. Part II: Application. *J. Atmos. Sci.,* **36,** 1072–1083.
——, and D. M. Byrne, 1976: A method for inferring total ozone content from the spectral variation of total optical depth obtained with a solar radiometer. *J. Atmos. Sci.,* **33,** 2242–2251.
——, and B. M. Herman, 1979: Determination of the ground albedo and the index of absorption of atmospheric particulates by remote sensing. Part I: Theory. *J. Atmos. Sci.,* **36,** 163–173.
——, D. M. Byrne, B. M. Herman, and J. A. Reagan, 1978: Aerosol size distributions obtained by inversion of spectral optical depth measurements. *J. Atmos. Sci.,* **35,** 2153–2167.
Lacis, A. A., B. E. Carlson, and B. Cairns, 1996: Multi-spectral atmospheric column extinction analysis of multi-filter rotating shadowband radiometer measurements. *Proc. Sixth Atmospheric Radiation Measurement (ARM) Science Team Meeting,* San Antonio, TX, Department of Energy, 145–148.
Leue, C., M. Wenig, T. Wagner, O. Klimm, U. Platt, and B. Jähne, 2001: Quantitative analysis of NO_x emissions from Global Ozone Monitoring Experiment satellite image sequences. *J. Geophys. Res.,* **106,** 5493–5505.
Meehl, G. A., W. M. Washington, D. J. Erickson III, B. P. Briegleb, and P. J. Jaumann, 1996: Climate change from increased CO_2 and direct and indirect effects of sulfate aerosols. *Geophys. Res. Lett.,* **23,** 3755–3758.
Mérienne, M. F., A. Jenouvrier, and B. Coquart, 1995: The NO_2 absorption spectrum I: Absorption cross-sections at ambient temperature in the 300–500-nm region. *J. Atmos. Chem.,* **20,** 281–297.
Michalsky, J. J., J. C. Liljegren, and L. C. Harrison, 1995: A comparison of sunphotometer derivations of total column water vapor and ozone to standard measures of same at the Southern Great Plains Atmospheric Radiation Measurement site. *J. Geophys. Res.,* **100,** 25 995–26 003.
——, L. Harrison, Q. Min, J. Schlemmer, W. Berkheiser II, and J. Berndt, 1996: Rotating shadowband spectroradiometer development and spectral shortwave data analysis progress. *Proc. Sixth Atmospheric Radiation Measurement (ARM) Science Team Meeting,* San Antonio, TX, Department of Energy, 209–212.
Mishchenko, M. I., L. D. Travis, R. A. Kahn, and R. A West, 1997: Modeling phase functions for dustlike tropospheric aerosols using a shape mixture of randomly oriented polydisperse spheroids. *J. Geophys. Res.,* **102,** 16 831–16 847.
Nakajima, T., G. Tonna, R. Rao, P. Boi, Y. Kaufman, and B. Holben, 1996: Use of sky brightness measurements from ground for remote sensing of particulate polydispersions. *Appl. Opt.,* **35,** 2672–2686.
Noxon, J. F., 1978: Tropospheric NO_2. *J. Geophys. Res.,* **83,** 3051–3057.
O'Neill, N. T., A. Royer, and J. R. Miller, 1989: Aerosol optical depth determination from ground-based irradiance ratios. *Appl. Opt.,* **28,** 3092–3098.
Pujadas, M., J. Plaza, J. Terés, B. Artiñano, and M. Millán, 2000:

Passive remote sensing of nitrogen dioxide as a tool for tracking air pollution in urban areas: The Madrid urban plume, a case of study. *Atmos. Eviron.,* **34,** 3041–3056.

Schmid, B., C. Mätzler, A. Heimo, and N. Kämpfer, 1997: Retrieval of optical depth and particle size distribution of tropospheric and stratospheric aerosols by means of sun photometry. *IEEE Trans. Geosci. Remote Sens.,* **35,** 172–181.

——, P. R. Spyak, S. F. Biggar, C. Wehrli, J. Sekler, T. Ingold, C. Mätzler, and N. Kämpfer, 1998: Evaluation of the applicability of solar and lamp radiometric calibrations of a precision sun photometer operating between 300 and 1025 nm. *Appl. Opt.,* **37,** 3923–3941.

——, and Coauthors, 1999: Comparison of aerosol optical depth from four solar radiometers during the fall 1997 ARM intensive observation period. *Geophys. Res. Lett.,* **26,** 2725–2728.

Schneider, W., G. K. Moortgat, G. S. Tyndall, and J. P. Burrows, 1987: Absorption cross-sections of NO_2 in the UV and visible region (200–700 nm) at 298 K. *J. Photochem. Photobiol.,* **40,** 195–217.

Schroeder, R., and J. A. Davies, 1987: Significance of nitrogen dioxide absorption in estimating aerosol optical depth and size distributions. *Atmos.–Ocean,* **25,** 107–114.

Shaw, G. E., 1976: Nitrogen dioxide—Optical absorption in the visible. *J. Geophys. Res.,* **81,** 5791–5792.

——, 1979a: Atmospheric ozone: determination by Chappuis-band absorption. *J. Appl. Meteor.,* **18,** 1335–1339.

——, 1979b: Aerosols at Mauna Loa: Optical properties. *J. Atmos. Sci.,* **36,** 862–869.

——, 1979c: Inversion of optical scattering and spectral extinction measurements to recover aerosol size spectra. *Appl. Opt.,* **18,** 988–993.

Slusser, J., J. Gibson, D. Bigelow, D. Kolinski, W. Mou, G. Koenig, and A. Beaubien, 1999: Comparison of column ozone retrievals by use of an UV multifilter rotating shadow-band radiometer with those from Brewer and Dobson spectrophotometers. *Appl. Opt.,* **38,** 1543–1551.

Smirnov, A., B. N. Holben, T. F. Eck, O. Dubovik, and I. Slutsker, 2000: Cloud-screening and quality control algorithms for the AERONET database. *Remote Sens. Environ.,* **73,** 337–349.

Soufflet, V., C. Devaux, and D. Tanre, 1992: Modified Langley plot method for measuring the spectral aerosol optical thickness and its daily variations. *Appl. Opt.,* **31,** 2154–2162.

Tanaka, M., T. Nakajima, and M. Shiobara, 1986: Calibration of a sunphotometer by simultaneous measurements of direct-solar and circumsolar radiations. *Appl. Opt.,* **25,** 1170–1176.

Tegen, I., A. A. Lacis, and I. Fung, 1996: The influence on climate forcing of mineral aerosols from disturbed soils. *Nature,* **380,** 419–422.

Teillet, P. M., 1990: Rayleigh optical depth comparisons from different sources. *Appl. Opt.,* **29,** 1897–1900.

Thomas, W., E. Hegels, S. Slijkhuis, P. Spurr, and K. Chance, 1998: Detection of biomass burning combustion products in Southeast Asia from backscatter data taken by the GOME spectrometer. *Geophys. Res. Lett.,* **25,** 1317–1320.

Wesely, M. L., 1982: Simplified techniques to study components of solar radiation under haze and clouds. *J. Appl. Meteor.,* **21,** 373–383.